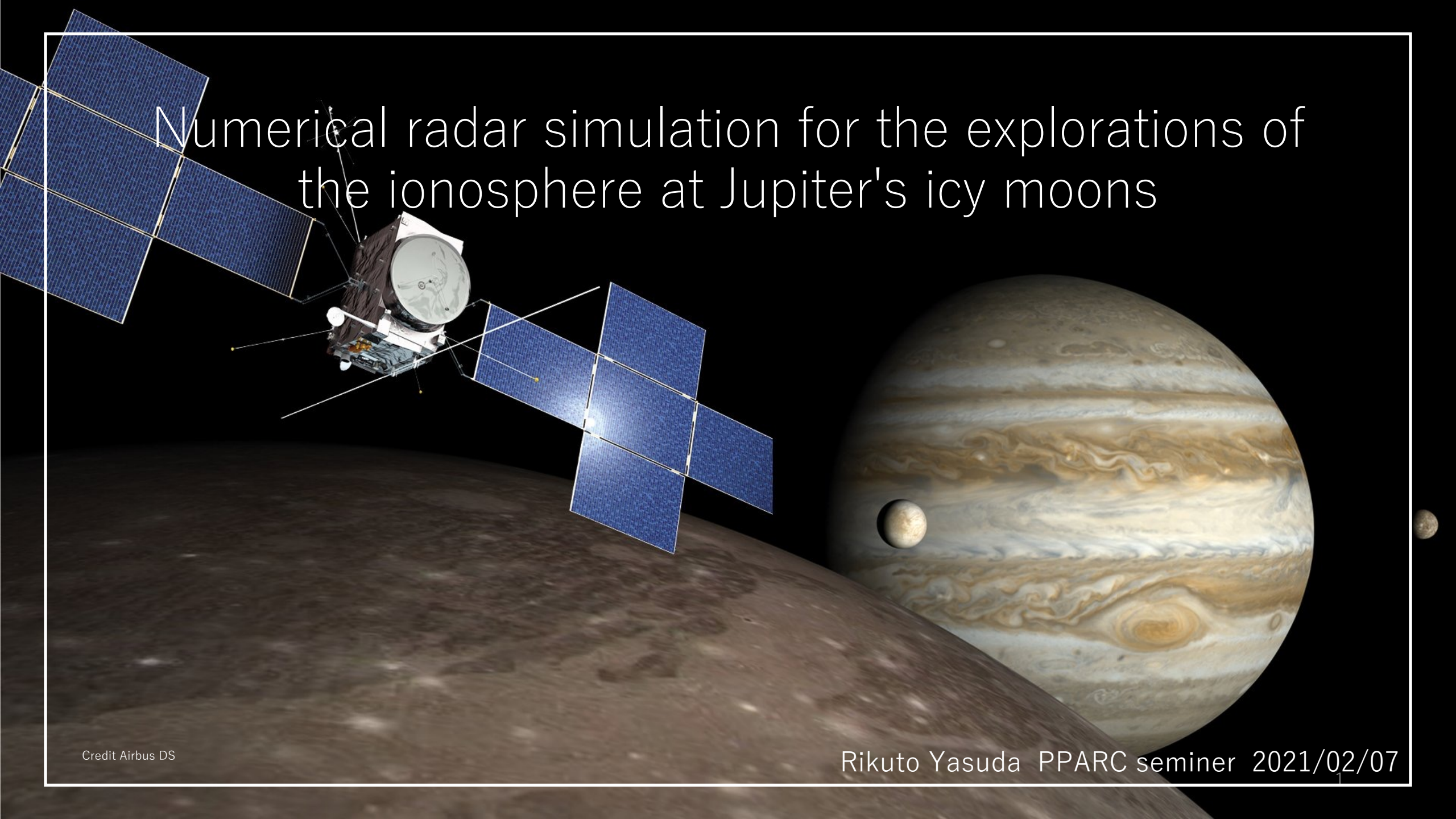


Numerical radar simulation for the explorations of the ionosphere at Jupiter's icy moons



1. Introduction

1-1 [Jupiter's icy moon](#)

1-2 [Ionosphere of Jupiter's icy moon](#)

1-3 Previous observation of moon's ionosphere electron density

[1-3-1 Ganymede ionosphere](#)

[1-3-2 Europa ionosphere](#)

[1-3-3 Calisto ionosphere](#)

[1-3-4 Problems with the previous observation methods](#)

1-4 [Preceding studies of Jovian radio emission occultations](#)

1-5 [Purpose of this study](#)

2. Method

2-1 ExPRES

2-2 How to combine Raytracing method
with Radio Emission Simulations

2-3 Raytracing

2-4 Verify time-step validity of raytracing code

3. Radio occultation observation

3-1 [Ganymede ionosphere model](#)

3-2 [Ganymede ionosphere result](#)

3-3 [Discussion](#)

4. Conclusion

5. Future works

Reference

Appendix

1-1. Jupiter's icy moon

~ Jupiter's icy moon ~

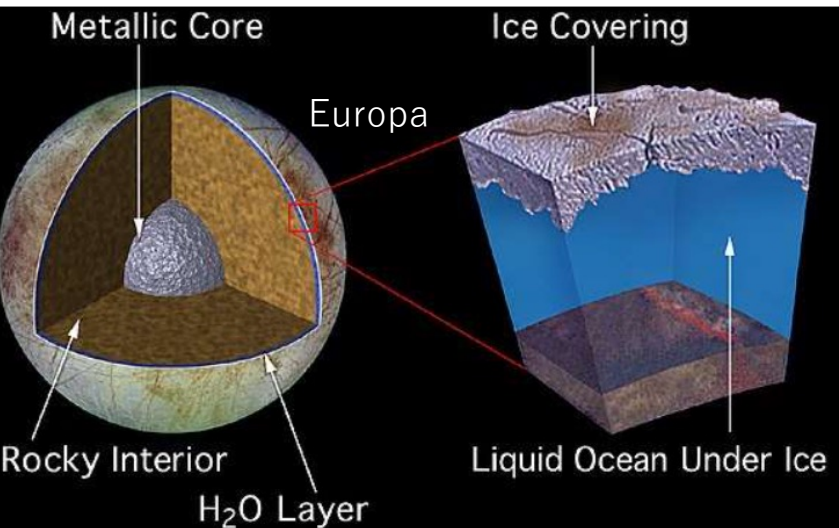
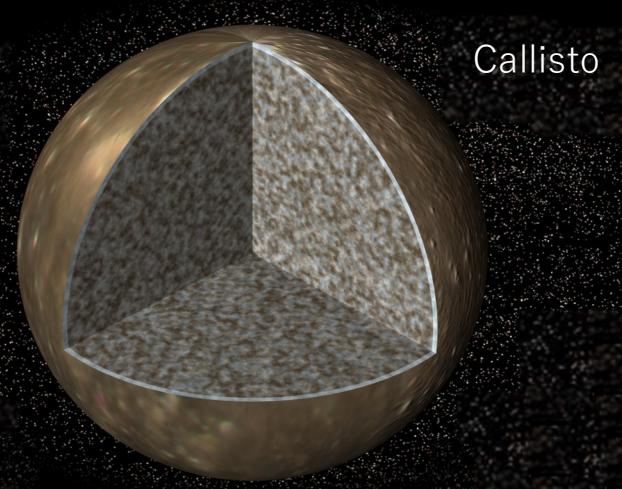
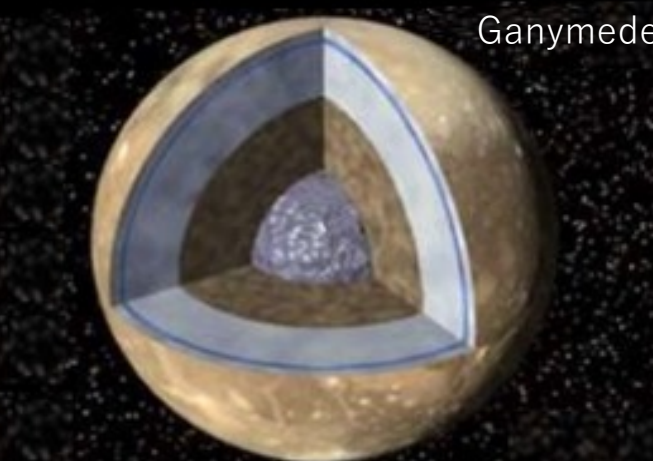


Fig.1 Model interiors of Ganymede Callisto and Europa [Schubert et al, 2004]

Jupiter's icy moon (ex. Europa, Ganymede, Callisto)

- possess internal liquid-water oceans [[Khurana et al., 1998](#); [Kivelson et al., 2002](#) etc..]
- Multiple icy bodies have subsurface ocean while only Earth has surface ocean.

Structures of the interior, ionosphere and plume of the icy moons are essential information for understanding universality of habitable environment.

It is impossible to observe directly ionosphere and plumes at low altitude as well as interiors.

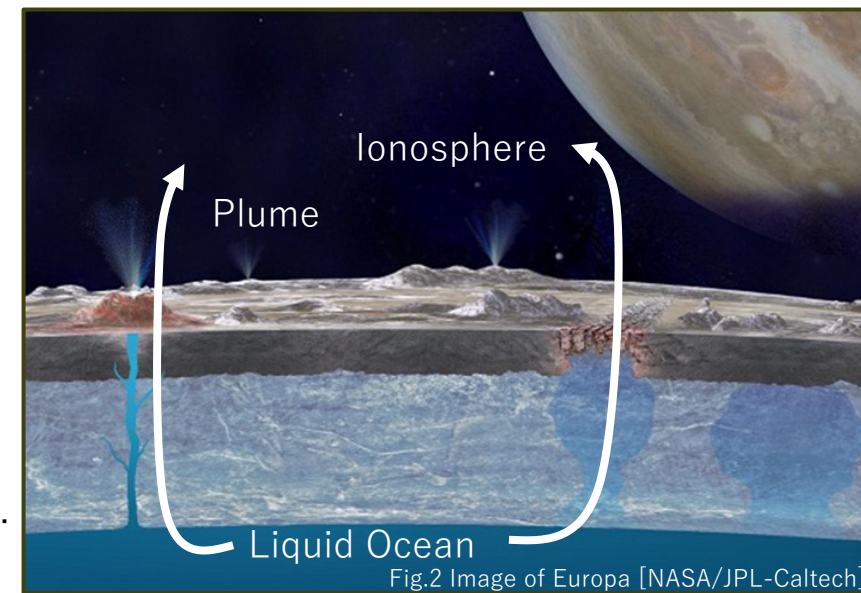


Fig.2 Image of Europa [NASA/JPL-Caltech]

1-1. Jupiter's icy moon

4

JUICE (JUpiter ICy moons Explorer)

Radio and Plasma Wave Investigation (RPWI) [Frequency: 80kHz~45MHz]

- ... A radio plasma wave instrument to characterize radio emission and plasma environment
- Apply to radio occultation observation or passive radar. (Fig.4, 5)



Fig.3 JUICE [Airbus DS]

① Radio occultation observation of the ionosphere

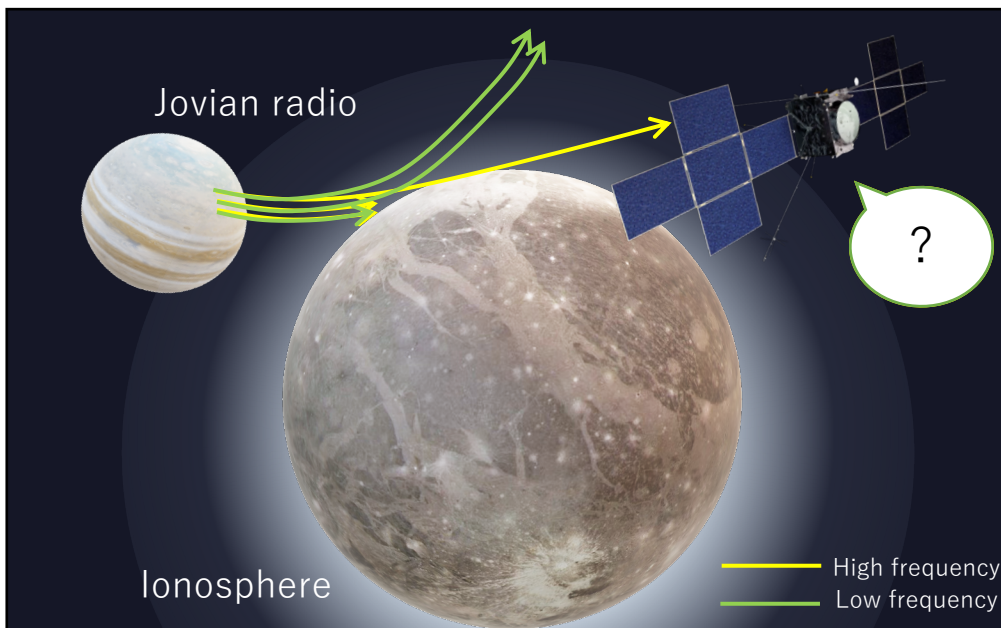


Fig.4 Radio observation using Jovian radio refraction
(adapted from Airbus DS and NASA/JPL)

② Passive radar

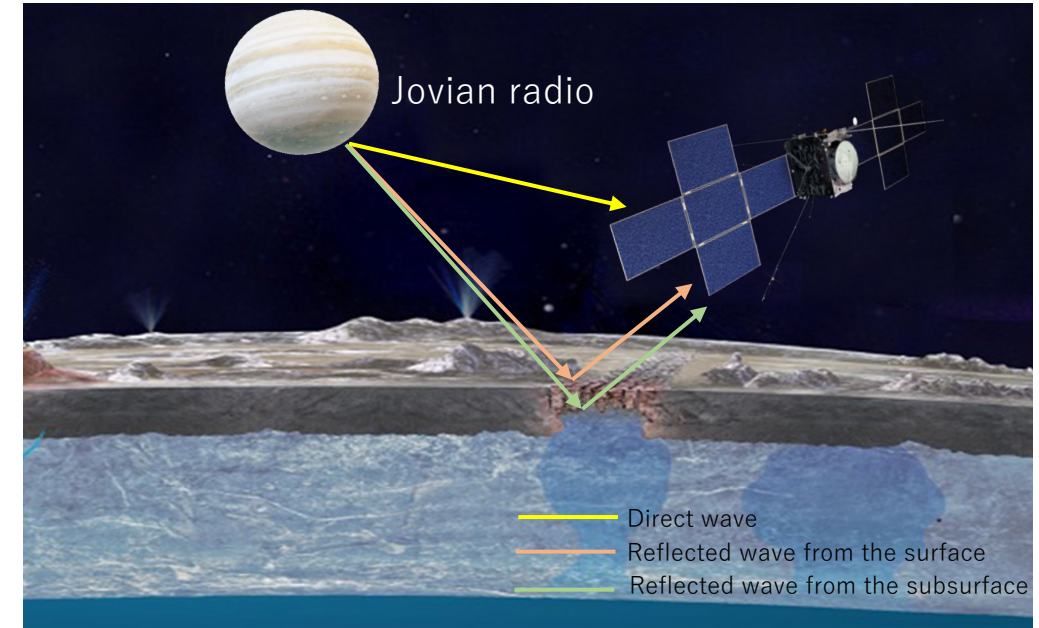
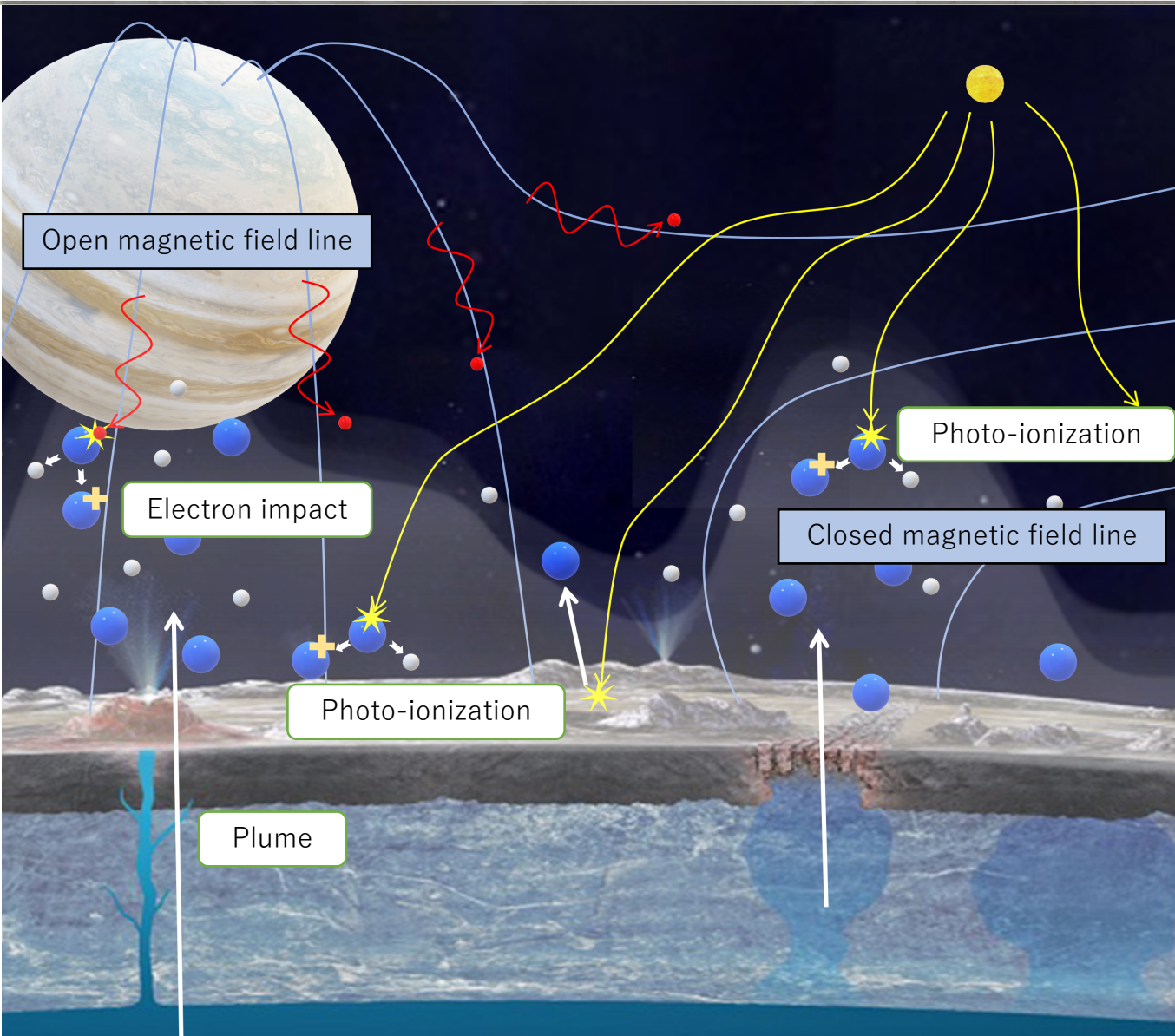


Fig.5 Radio observation using Jovian radio reflection
(adapted from NASA/JPL, Airbus DS and gcoe-earths.org)

1-2. Ionosphere of Jupiter's icy moon



Ionization source ([Carnielli et al. \(2019\)](#))

① Photo-ionization

exosphere is constantly photo-ionized by solar EUV radiation

② Electron impact

the energetic electrons (> tens of eV) are able to ionize the neutral exosphere.

Ionosphere structure of icy moons

- Distribution of neutral atmosphere (and plume) created from oceanic water materials
- Solar photo-ionization rate and electron impact ionization rate (Energy sources into icy moon)
- Open or closed magnetic field line (Ganymede)

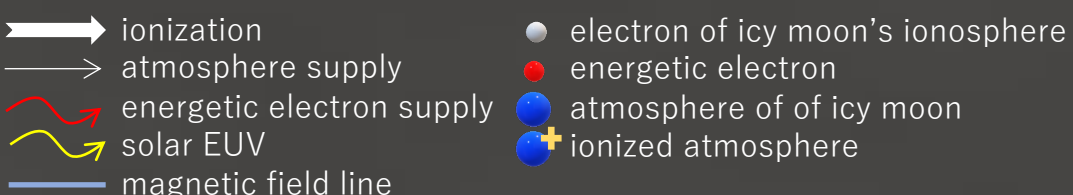


Fig. Ionization process of icy moon
(adapted from NASA/JPL, Airbus DS and gcoe-earths.org)

1-3. Previous observation of moon's ionosphere electron density

6

1-3-1. Ganymede ionosphere

In-situ observation of Galileo flyby [Galileo plasma-wave instrument] (Fig.)

Upper hybrid resonance frequency $f_{UH} = \sqrt{f_p^2 + f_c^2}$

When $f_{UH} \gg f_c$, $f_{UH} = f_p = 8980\sqrt{N}$ (Hz)

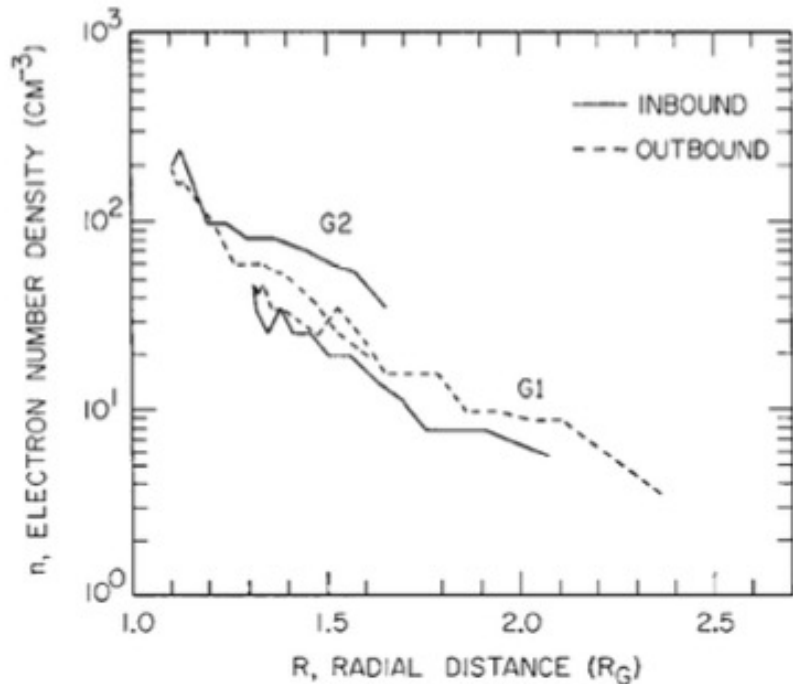


Fig. Electron density profiles on Ganymede 2 obtained by means of the PWS instrument on Galileo (Eviatar et al. 2001a)

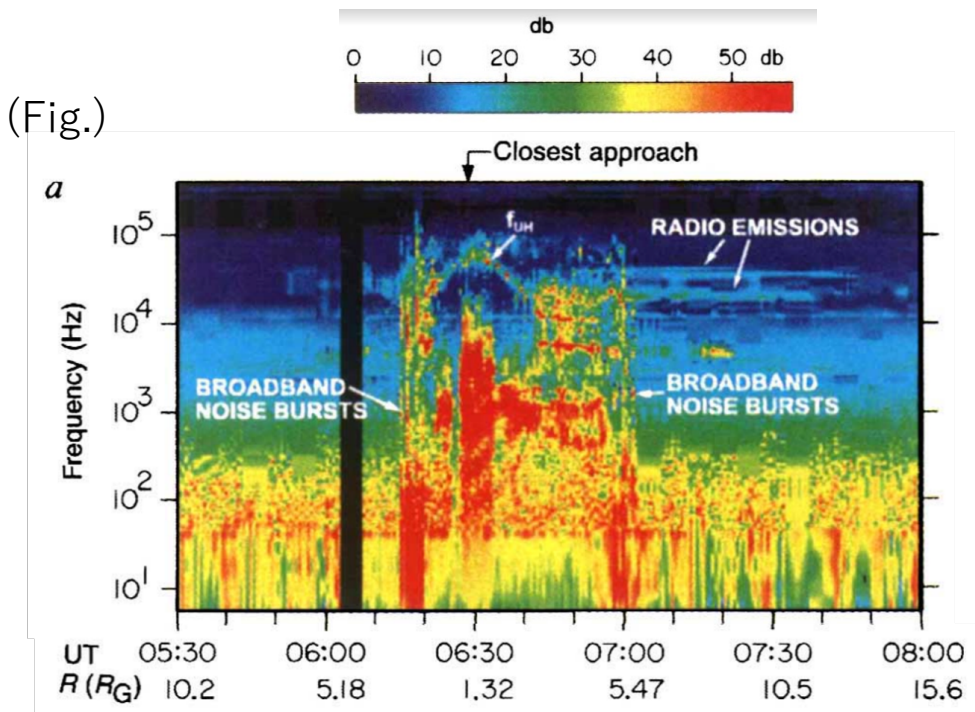


Fig. Frequency-time spectrograms of the electric field intensities detected by Galileo plasma wave instrument during the 27 June 1996 Ganymede fly-by (Eviatar et al. 2001a)

	Maximum densities	Scale height	
Gurnett et al. 1996	~ 100 (/cc)	~1000 km	G1
Eviatar et al. 2001a	~ 400 (/cc)	~600 km	G1&G2
Eviatar et al. 2001b	~ 2500 (/cc)	~125km (near Ganymede) ~600 km (farther out)	G2

Fig. Proposed maximum electron densities and scale height of Ganymede ionosphere

1-3. Previous observation of moon's ionosphere electron density

7

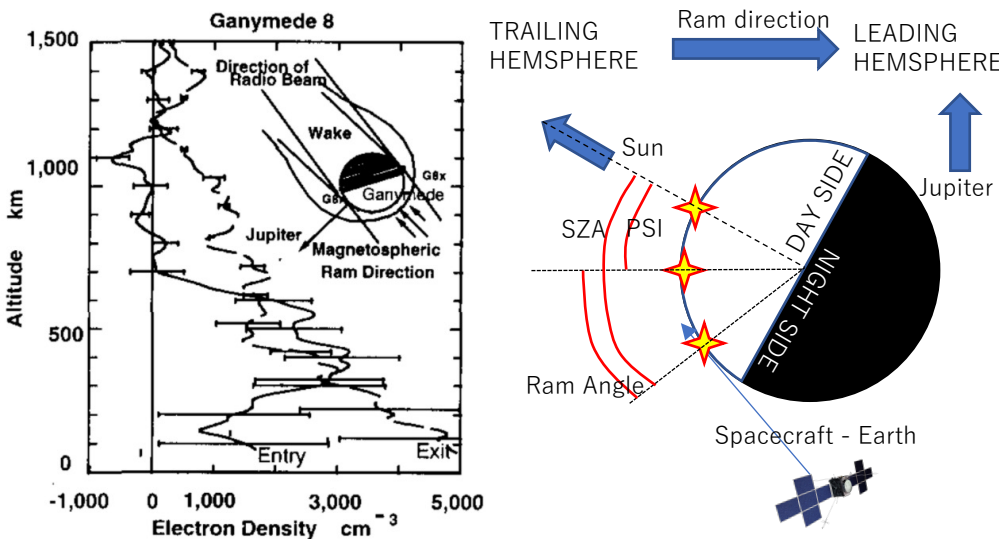
1-3-1. Ganymede ionosphere

Radio occultation [Galileo]

Maximum electron densities ... $\sim 4000/\text{cc}$ ([Kliore 1998](#))

Observation	Lat (deg)	W. Long (deg)	SZA (deg)	Ram Angle (deg)
Ganymede 8 entry	41	201	82	69
Ganymede 8 exit	47	22	98	112

Fig. Geometry of Galileo occultations by Ganymede.



Only one strong detection ([McGrath et al. \(2004\)](#))

(strong detection 1/8 weak detection 2/8 non-detecton 5/8)

(The ionospheres of Ganymede and Callisto from Galileo radio occultations)

Fig. Electron density profiles for Ganymede
([Kliore 1998](#))

Fig. Ram angle, SZA and PSI

[Carnielli et al. \(2019\)](#)

- ~ ([Eviatar et al., 2001](#)) presented electron density profiles from the Plasma Wave Science (PWS) instrument along the G1 and G2 flyby trajectories, consistent with the upper limit of [Kliore \(1998\)](#). ~
- ~ in the region of closed magnetic field lines we would expect mainly low energy electrons to be present from photo-ionization of the neutral atmosphere, and not energetic electrons from the Jovian plasma sheet which are not able to penetrate ~



Electron density distribution of ionosphere → What is the origin of Ganymede ionosphere?

1-3. Previous observation of moon's ionosphere electron density

1-3-2. Callisto ionosphere

Radio occultation [Galileo] ([Kliore et al. 2002](#))

Maximum electron densities

- ... $15300 \pm 2300/\text{cc}$ (C22 entry • peak altitude $\sim 27\text{km}$)
- $17400 \pm 1500/\text{cc}$ (C23 entry • peak altitude $\sim 48\text{km}$)

Observation	Lat (deg)	SZA (deg)	Ram (deg)	Psi (deg)	detection
C9 entry	2.2	81.5	105.7	172.9	none
C9 exit	2.8	98.5	74.4	//	none
C20 entry	8.6	85.0	82.8	2.4	weak+
C20 exit	0.8	101.3	99.2	//	weak+
C22 entry	3.6	78.7	80.9	2.1	strong++
C22 exit	7.5	95.0	97.8	//	weak+
C23 entry	6.6	82.5	81.7	1.0	strong++
C23 exit	3.6	97.6	98.9	//	weak+

Fig. Geometry of Galileo occupations by Callisto.

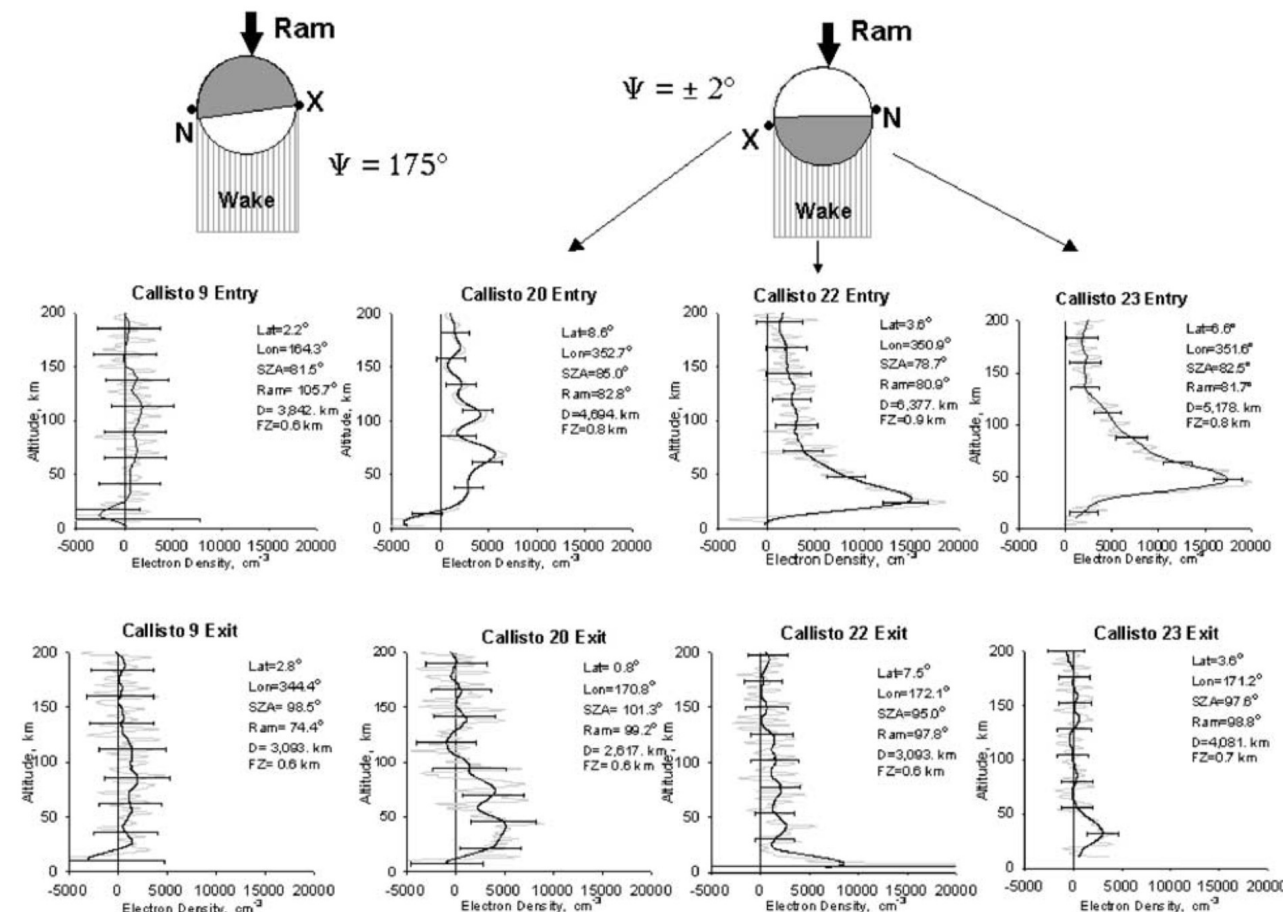


Fig. Electron density profiles for Callisto (Kliore et al. 2002)

It was found that the presence of a detectable ionosphere, at least in the equatorial terminator regions, coincided **with solar illumination of the trailing hemisphere** of Callisto.

1-3. Previous observation of moon's ionosphere electron density

1-3-2. Callisto ionosphere

In-situ observation of Galileo flyby [Galileo plasma-wave instrument]

Maximum electron densities ... $\sim 400/\text{cc}$ C10 flyby • closest approach altitude 535km

([Gurnett et al](#) (2000))

$\sim 100/\text{cc}$ C3 flyby • closest approach altitude 1136km

([Gurnett et al](#) (1997))

Date	96/11/04	97/06/25	97/09/17	99/05/05	99/06/30	99/08/14	99/09/16	01/05/25
Flyby-No.	C3	C9	C10	C20	C21	C22	C23	C30
Magnetic	✓	✓	✓	x	✓	✓	✓	✓
Radio	x	✓	x	✓	x	✓	✓	x
Up/Down	Down	Up	Down	Down	Down	Down	Down	Down
Day/Night	Day	Night	Day	Night	Both	Night	Night	Both
C/A [km]	1136	418	535	1321	1048	2299	1052	132
$h_{CS} [R_J]$	3.24	-3.52	-2.45	2.93	-1.87	-4.31	1.08	3.50

Fig. Date of flyby (Date), flyby identification number (Flyby-No.), magnetometer measurement (Magnetic), radio occultation measurement (Radio), flyby passing the upstream or/and downstream side (Up/Down), flyby passing the day or/and night side (Day/Night), closest approach altitude (C/A), distance from the magnetospheric current sheet (h_{CS}). ([Hartkorn](#) (2017))

[Gurnett et al](#) (2000)

- The closest approaches for C3 and C10, which had the highest plasma densities, were on the sunlight side of the moon
- the closest approach for C22, which had very low plasma densities, was on the dark side of the moon

This local time dependence could indicate that solar illumination plays a role in controlling the plasma density.

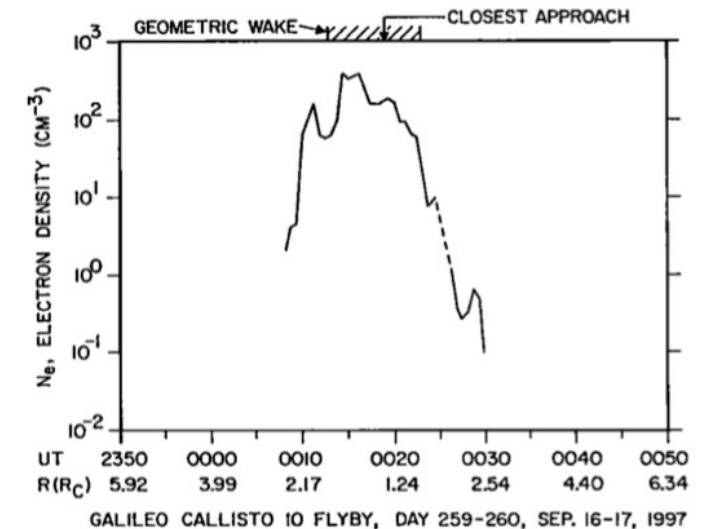


Fig. Electron density profiles determined from the upper hybrid resonance frequency during the C10 flyby. ([Gurnett et al.](#) (2000))

1-3-3. Europa ionosphere

Radio occultation [Galileo] ([Kliore et al. \(1997\)](#))

Maximum electron densities ... $9000 \pm 4000/\text{cc}$

Scale height ... $240 \pm 40 \text{ km} (\sim 300 \text{ km})$
 $440 \pm 60 \text{ km} (300 \text{ km} \sim)$

Strong detection ... 5 times

Weak detection ... 1 times

Non_detection ... 2 times

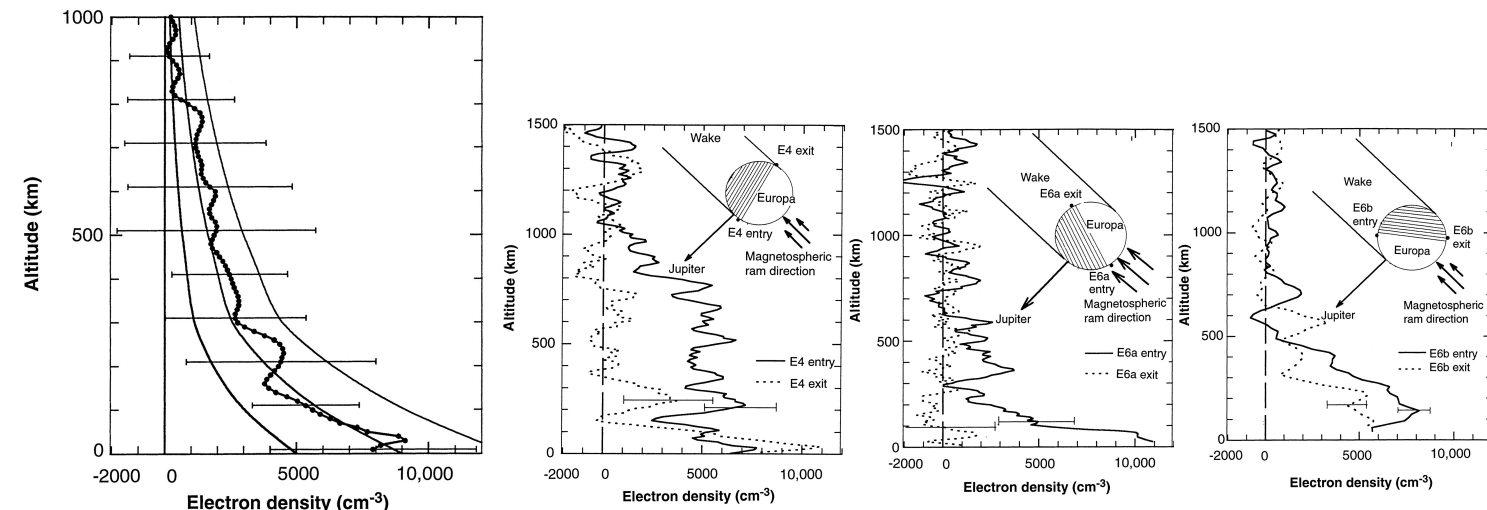


Fig. Average Europa electron density profile computed from the five observations in which an ionosphere was detected.(Kliore et al. 1997)

Fig. Electron density profiles for Europa. (E4, E6a and E6b) (Kliore et al. 1997)

[Kliore et al. \(2001\)](#)

- in order for an ionosphere to be observed, the trailing hemisphere of the satellite **must be in sunlight**
- the atmosphere created by sputtering effects of the Jovian magnetosphere can be **ionized by solar EUV to produce an observable ionosphere.**



- the electron impact ionization rate is $1.9 \times 10^{-6} \text{ s}^{-1}$ & a solar maximum photoionization rate is $3 \times 10^{-8} \text{ s}^{-1}$ ([Saur et al. \(1998\)](#))
- It is therefore very difficult to understand why the existence of an ionosphere should depend on solar illumination. ([McGrath et al. \(2009\)](#))

1-3-3. Europa ionosphere

In-situ observation of Galileo flyby [Galileo plasma-wave instrument] (Fig.)

The maximum density enhancement observation on any flyby

… $600 \text{ (cm}^{-3})$ at E12 flyby ([Kurth et al. \(2001\)](#))

The maximum density enhancement observation as the spacecraft entered the wake.

… $200 \text{ (cm}^{-3}) \Rightarrow 400 \text{ (cm}^{-3})$ at E15 flyby ([McGrath et al. \(2009\)](#))

Flyby	Time of closest approach	Alt. (km)	Upstream/ wake	Magnetic latitude ($^{\circ}$)	λ_{III} ($^{\circ}$)	LT ^a (h)	Day/night	Jupiter/Anti-ju hemisphere
E4	Dec. 19, 1996 0652:58	692	Wake	6.6	157	16.7	Night	Jupiter
E6	Feb. 20, 1997 1706:10	586	Upstream	-7.6	340	12.9	Night	Jupiter
E11	Nov. 6, 1997 2031:44	2043	Wake	8.7	223	11.0	Day	Anti-Jupiter
E12	Dec. 16, 1997 1203:20	201	Upstream	0.9	118	14.7	Day	Anti-Jupiter
E14	Mar. 29, 1998 1321:05	1644	Upstream	9.1	184	14.4	Day	Anti-Jupiter
E15	May 31, 1998 2112:57	2515	Wake	-0.5	293	10.1	Day	Anti-Jupiter
E17	Sep. 26, 1998 0354:20	3582	Wake	3.6	138	9.9	Day	Anti-Jupiter
E19	Feb. 1, 1999 0219:50	1439	Upstream	5.6	256	9.8	Night	Jupiter
E26	Jan. 3, 2000 1759:43	198	Flux tube	-9.6	2	2.9	Night	Jupiter

^aLocal time with respect to Jupiter.

Fig. Galileo Europa flyby geometric. ([Kurth et al. \(2001\)](#))

The origin and characteristics of Europa ionosphere are still very poorly understood.

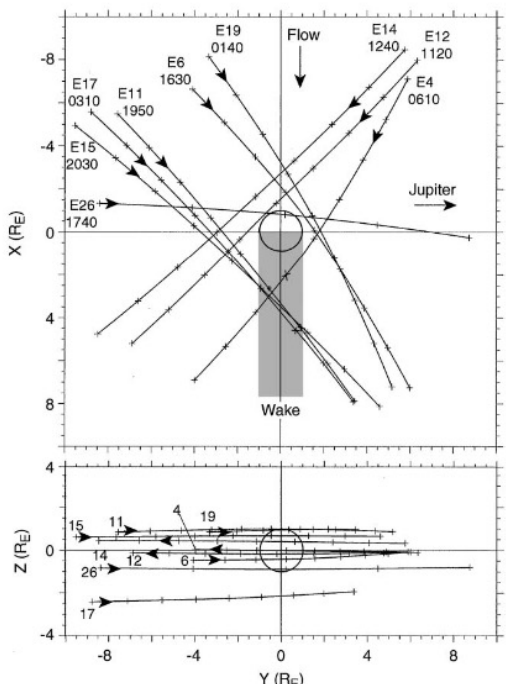


Fig. The geometry of nine Galileo flybys of Europa. ([Kurth et al. \(2001\)](#))

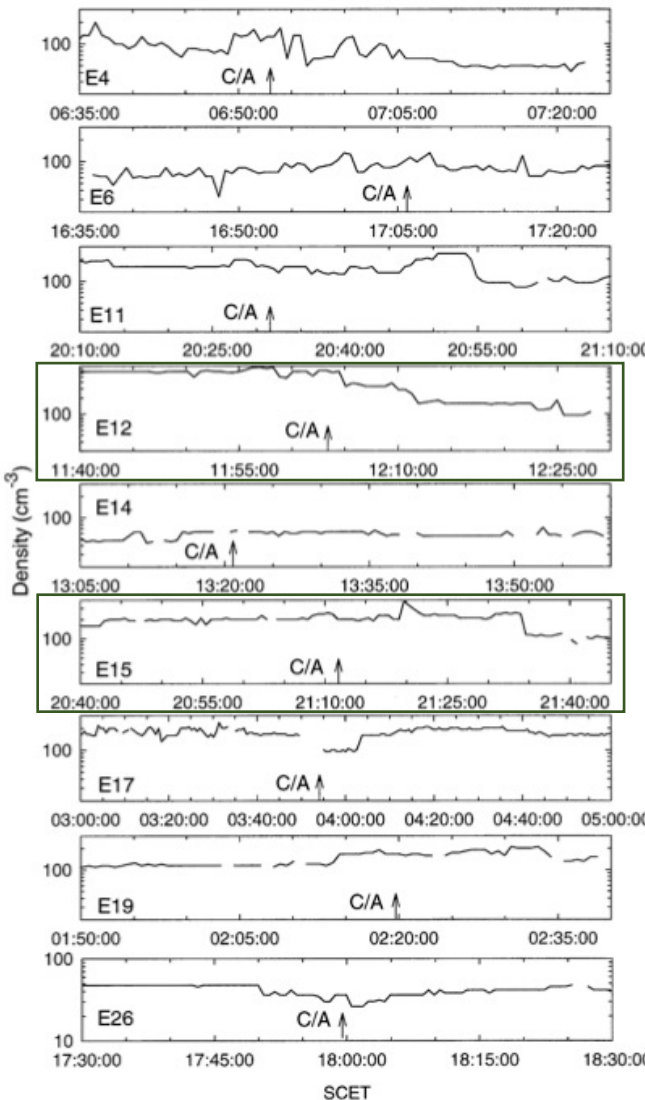
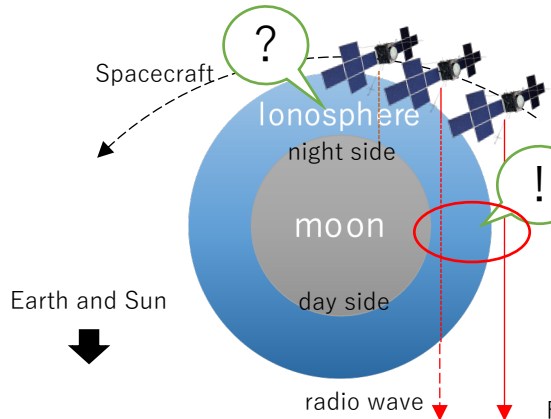


Fig. Electron density profiles based on the upper hybrid resonance band observed during each of Europa flyby. ([Kurth et al. \(2001\)](#))

1-3-4. Problems with the previous observation methods

Radio occultation

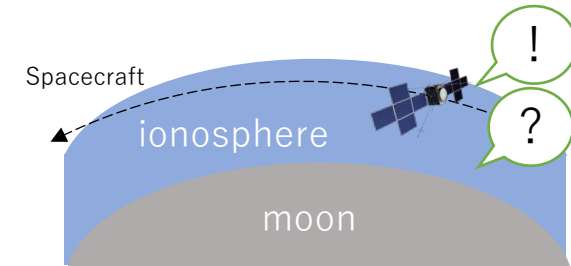


Only ionosphere
around day–night boundary

- difficult to evaluate photo-ionization process
- difficult to detect the differences between leading and trailing hemisphere (depend on the positions of the moon, Jupiter and sun)

Fig. Radio observation using spacecraft radio

In-situ observation

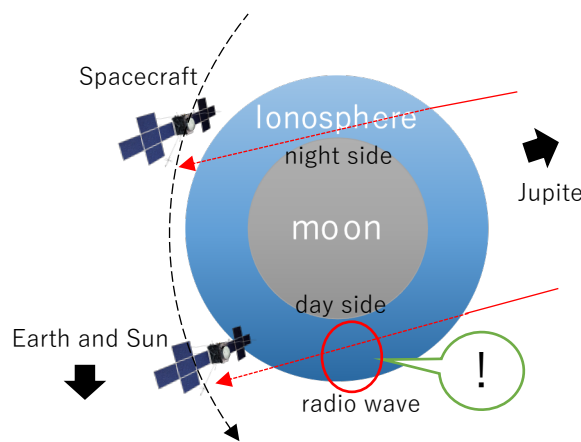


Lack of information
at low altitude

- difficult to measure the vertical ionospheric profiles

Fig. In-situ observation

Jovian radio occultation



Contribute to ...

- estimate the distribution of neutral atmosphere (and plume)
- identify what the origin of icy moons' ionosphere is

Fig. Radio observation using jovian radio

Occultation modeling using ExPRES Jovian Radio Emission Simulations [Cecconi et al, 2021]

※ Assuming a straight-line propagation (no refraction)

- At lower frequencies, the occultation spectral egress occurs later than predicted. (Fig. 10)
- This prediction mismatch indicates that propagation effects play an important role in the fine understanding of the radio occultation near Galilean moons.

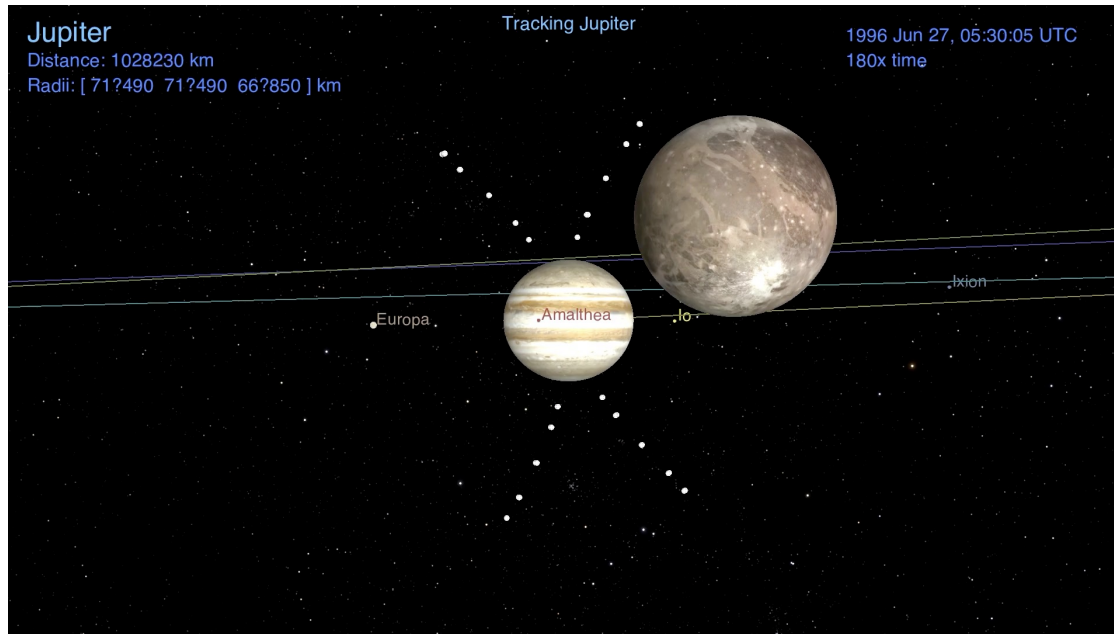


Fig.9 Flyby visualized in the Cosmographia tool. The scene is set with an observer on the Galileo spacecraft, pointing to Jupiter. Ganymede is in the field of view. The ExPRES-modelled visible radio sources are also shown, at 700 kHz, 1 MHz, 2 MHz, 5 MHz and 10 MHz as white dots. The radio sources are conventionally grouped in four sets (named A, B, C and D). [Cecconi et al, 2021]

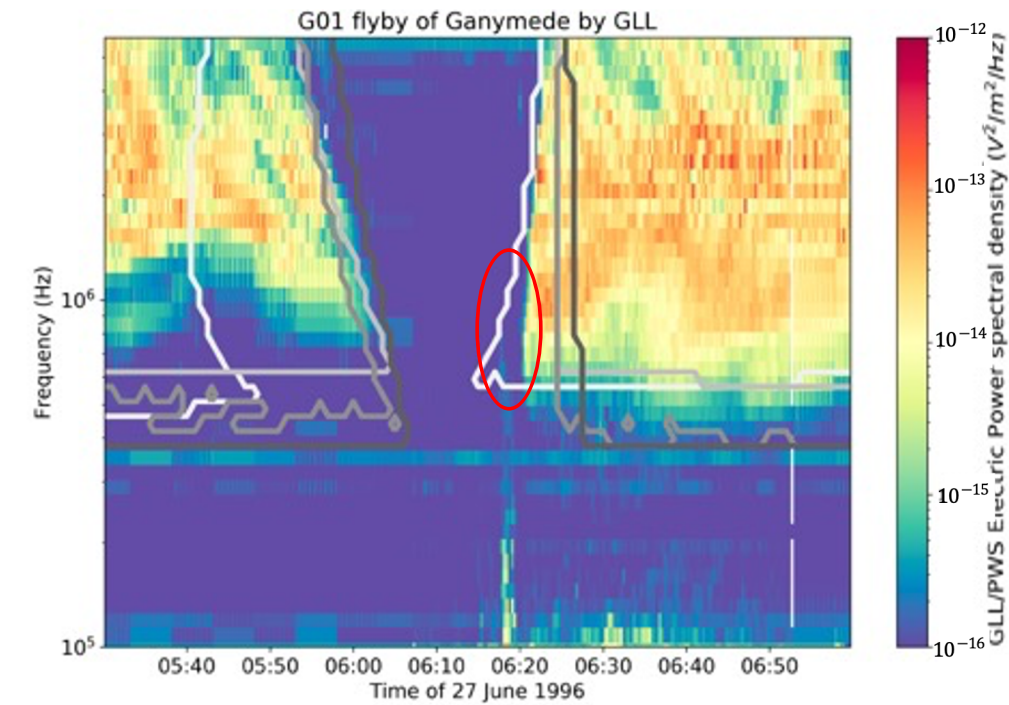


Fig.10 Superimposed Galileo PWS data and ExPRES simulations during Jovian radio emission occultations by Ganymede . The four types of emission (A, B, C, D) are separated (from white to darkgrey, resp.) [Cecconi et al, 2021]

- To investigate spatial structures of ionosphere and plumes created from the water oceanic materials, developing the numerical simulation code for the radar explorations using natural radio waves. [Fig. 4]
(Collaborative research with institutions in France and Sweden)
- Finally, we will also investigate spatial structures of the interior. [Fig. 5]



① Radio occultation observation

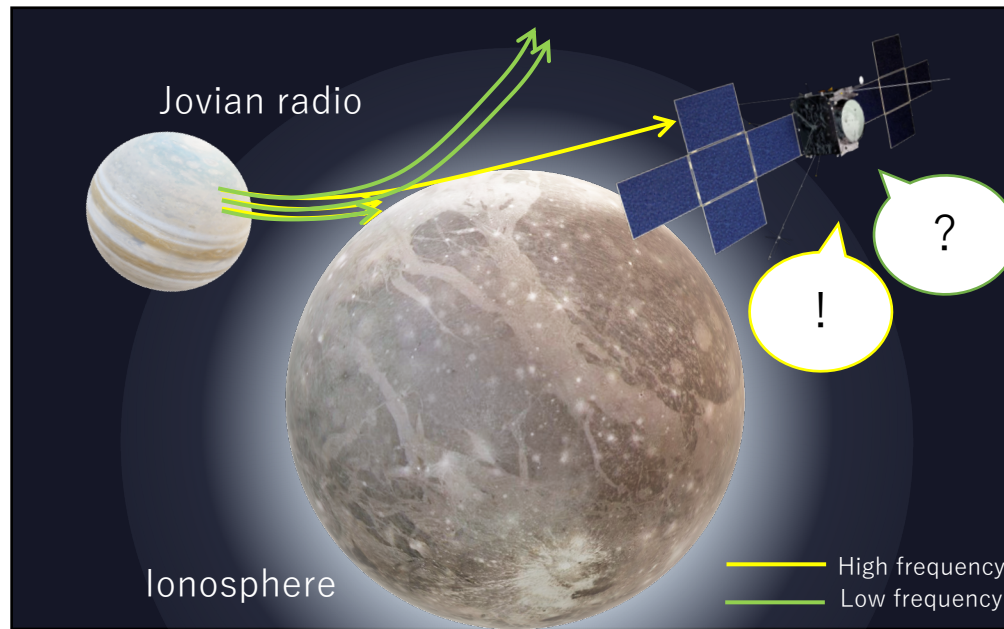


Fig.4 Radio observation using Jovian radio refraction (adapted from Airbus DS and NASA/JPL)

② Passive radar

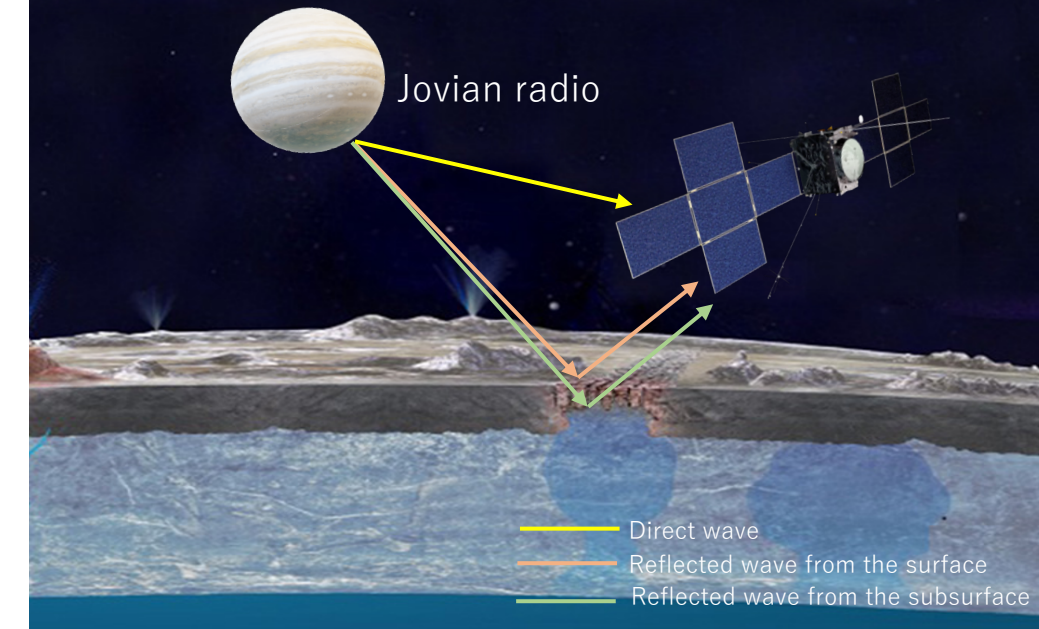


Fig.5 Radio observation using Jovian radio reflection (adapted from NASA/JPL, Airbus DS and gcoe-earths.org)

Today's topic..

- Emulate occultation of the Jovian radio waves during the flybys of the Galileo spacecraft to Ganymede including the ionospheric refraction effect**
- Propose the vertical ionospheric profiles at the altitude below the orbiter**

6. Reference

- Aharon Eviatar, Vytenis M. Vasyliūnas, Donald A. Gurnett (2001), The ionosphere of Ganymede, Planetary and Space Science Volume 49, Issues 3–4, March 2001, Pages 327–336
- B. Cecconi, C. K. Louis, C. Muñoz Crego, and C. Vallat (2021), Auroral Radio Source Occultation Modeling and Application to the JUICE Science Mission Planning
- Kazuo Ouchi (2017), Principles of Radar - From Search Radar to Synthetic Aperture Radar, Publisher: Corona Publishing Co.
- Kimura, T., F. Tsuchiya, H. Misawa, A. Morioka, and H. Nozawa (2008a), Occurrence and source characteristics of the high - latitude components of Jovian broadband kilometric radiation, *Planet. Space Sci.*, **56**, 1155– 1168, doi:[10.1016/j.pss.2008.03.001](https://doi.org/10.1016/j.pss.2008.03.001).
- Paterson, W. R., Frank, L. A. Ackerson, K. L (1997), Galileo plasma observations at Europa: Ion energy spectra and moments, Journal of Geophysical Research, Volume 104, Issue A10, p. 22779-22792, doi:10.1029/1999JA900191
- Xianzhe Jia, Margaret G. Kivelson, Krishan K. Khurana and William S. Kurth (2018), Evidence of a plume on Europa from Galileo magnetic and plasma wave signatures, *Nature Astronomy* 2, 459–464 (2018),
- Kliore, A. J., Anabtawi, A. Nagy, A. F.; Galileo Radio Propagation Science Team (2001), The ionospheres of Ganymede and Callisto from Galileo radio occultations, *Bulletin of the American Astronomical Society*, Vol. 33, p.1084 DOI: 10.1038/s41550-018-0450-z
- M. A. McGrath, C. J. Hansen, A. R. Hendrix, Kurt Retherford (2009), Observations of Europa's Tenuous Atmosphere, *Europa*.
- MASER HP <https://maser.lesia.obspm.fr/publications/doi/auroral-radio-source-occultation.html?lang=en#G01> (2021/5/2)
- NASA HP <https://www.nasa.gov/topics/solarsystem/features/pia16826.html> (2021/5/2)
- GCOE HP <https://www.gcoe-earths.org/en/jupiter.html> (2021/5/2)
- McGrath, Melissa A.; Lellouch, Emmanuel; Strobel, Darrell F.; Feldman, Paul D.; Johnson, Robert E. (2004), Satellite atmospheres, *Jupiter*
- Hartkorn, Oliver, 2017. Modeling Callisto's Ionosphere, Airglow and Magnetic Field Environment. Technical Report. Köln Universitat.
- Khurana, K., Kivelson, M., Stevenson, D. *et al.* Induced magnetic fields as evidence for subsurface oceans in Europa and Callisto. *Nature* 395, 777–780 (1998).
- M.G. Kivelson, K.K. Khurana, M. Volwerk (2002), The permanent and inductive magnetic moments of Ganymede, *Icarus*, 157, pp. 507–522
- Schubert et al. (2004). Interior, composition, structure and dynamics of the Galilean satellites, in *Jupiter. The planet, satellites and magnetosphere*, Cambridge University Press
- D.A. Gurnett, W. S. Kurth, A. Roux, S.J. Bolton & C.F. Kernel (1996), Evidence for a Magnetosphere at Ganymede from Plasma-wave Observations by the Galileo Spacecraft. *Nature* 384(6609) doi: 10.1038/384535a0
- Eviatar, A., Vasyliūnas, M. V., & Gurnett, A. D. (2001a). The ionosphere of Ganymede. *Planetary and Space Science*, 49(3), 327–336. <https://doi.org/10.1016/S0032-0633%2800%2900154-9>
- Aharon Eviatar, Darrell F. Strobel, Brian C. Wolven, Paul D. Feldman, Melissa A. McGrath, and Donald J. Williams (2001b), Excitation of the Ganymede Ultraviolet Aurora. *THE ASTROPHYSICAL JOURNAL*, 555 : 1013È1019, 2001 July 10
- G. Carnielli, M. Galand, F. Leblanc, L. Leclercq, R. Modolo, A. Beth, H.L.F. Huybrighs, X. Jia (2019), First 3D test particle model of Ganymede's ionosphere, *Icarus* Volume 330, 15 September 2019, Pages 42–59 <https://doi.org/10.1016/j.icarus.2019.04.016>
- A. J. Kliore, A. Anabtawi, R. G. Herrera, S. W. Asmar, A. F. Nagy, D. P. Hinson, and F. M. Flasar (2002), Ionosphere of Callisto from Galileo radio occultation observations, *JOURNAL OF GEOPHYSICAL RESEARCH*, VOL. 107, NO. A11, 1407, doi:10.1029/2002JA009365, 2002
- D. A. Gurnett, A.M. Persoon, W. S. Kurth (2000), Plasma densities in the vicinity of Callisto from Galileo plasma wave observations, *GEOPHYSICAL RESEARCH LETTERS*, VOL. 27, NO. 13, PAGES 1867–1870, JULY 1, 2000
- D. A. Gurnett, W. S. Kurth, A Rouxt & S. J. Bolton (1997), Absence of a magnetic-field signature in plasma-wave observations at Callisto, *NATURE* | VOL 387 | 15 MAY 1997
- A. J. Kliore, D. P. Hinson, F. M. Flasar, A. F. Nagy, T. E. Cravens (1997), The Ionosphere of Europa from Galileo Radio Occultations, *Science* 18 Jul 1997: Vol. 277, Issue 5324, pp. 355–358 DOI: 10.1126/science.277.5324.355
- Kliore, A. J.; Anabtawi, A.; Nagy, A. F (2001), The Ionospheres of Europa, Ganymede, and Callisto American Geophysical Union, Fall Meeting 2001, abstract id.P12B-0506
- W.S. Kurth; D.A. Gurnett, A.M. Persoon, A. Roux, S.J. Bolton, C.J. Alexander (2001), The plasma wave environment of Europa, *Planetary and Space Science* 49 (2001) 345–363

- In numerical radar simulation, full wave simulation is general method.

ex) FDTD (Finite-difference time-domain method) method (Fig.13) Δz
 ... Solving Maxwell's equations on a mesh and computing E and H
 at grid points spaced Δx , Δy , and Δz apart.

- However, this method needs high calculation cost when we execute the program in a wide calculation space such as ionosphere, plumes and interiors of icy moons.

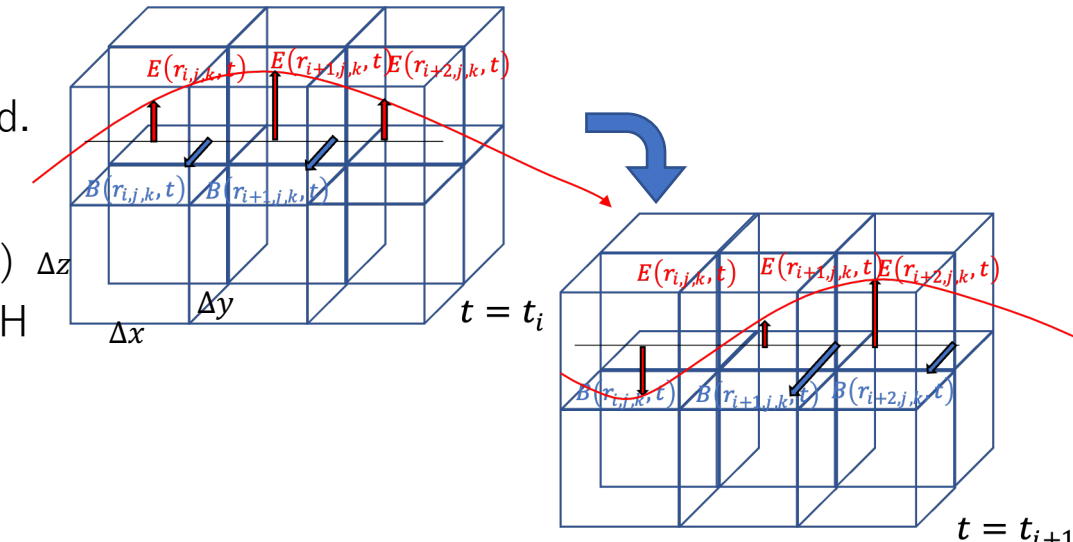


Fig.13 FTDT image

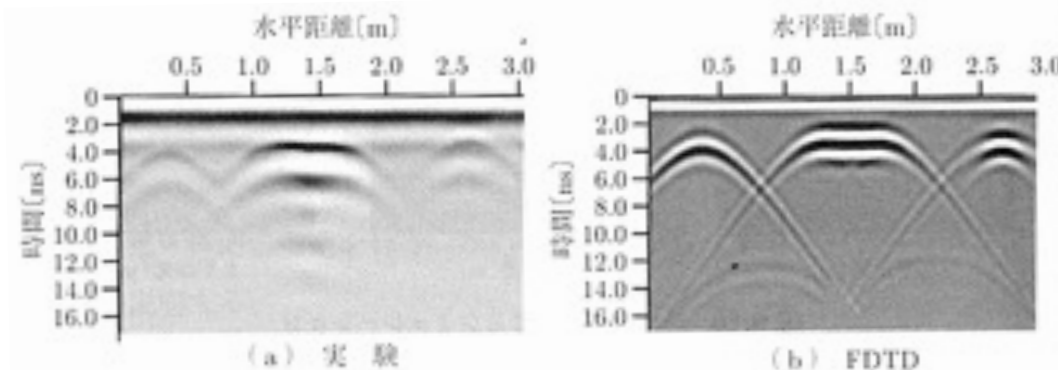


Fig.14 FTDT result [Principles of radar (Kazuo Ouchi)]

Ray tracing ..

more computationally efficient to trace propagation paths of electromagnetic waves in the magnetized plasma, sequentially solving the dispersion relation for plasma waves.

~ input parameter ~

- Magnetic field model $\omega_c(\vec{r}, t)$
- Plasma density model $\omega_p(\vec{r}, t)$
- Frequency of wave (ω)
- Initial position (\vec{r}_0)
- Initial wave vector (\vec{k}_0)



$d\vec{r}_{j+1}$ and $d\vec{k}_{j+1}$ in dt_j

$$(1) \rightarrow d\vec{r}_{j+1} = -\frac{\partial D_j / \partial \vec{k}_j}{\partial D_j / \partial \omega} \cdot dt_j, \quad d\vec{k}_{j+1} = +\frac{\partial D_j / \partial \vec{r}_j}{\partial D_j / \partial \omega} \cdot dt_j$$



the time (t_{j+1}), position (\vec{r}_{j+1}) and wave vector (\vec{k}_{j+1}) after dt_j

- $t_{j+1} = t_j + dt_j$
- $\vec{r}_{j+1} = \vec{r}_j + d\vec{r}_{j+1}$
- $\vec{k}_{j+1} = \vec{k}_j + d\vec{k}_{j+1}$



~ output ~

a full ray path and time ($\vec{r}(t)$)

- Equation of motion of plasma

$$\frac{d\vec{v}}{dx} = \frac{q}{m} (\vec{E} + \vec{v} \times \vec{B})$$

- Maxwell's equations

$$\nabla \times \vec{H} = \vec{j} + \frac{\partial \vec{D}}{\partial t} \quad \nabla \times \vec{E} = -\frac{\partial \vec{B}}{\partial t}$$



(Cold plasma · Discarding plasma collision)

Appleton-Hartree equation (Cf. Appendix A)

~The dispersion relation of waves in magnetized cold plasma~

$$D(t, \vec{r}, \omega, \vec{k}) = \left(\frac{c|\vec{k}|}{\omega} \right)^2 + \frac{2X}{2 - \frac{Y^2 \sin^2 \theta}{1-X} + \rho \sqrt{\frac{Y^2 \sin^4 \theta}{(1-X)^2} + 4Y^2 \cos^2 \theta}} - 1 = 0 \quad \dots (1)$$

$$X = \left(\frac{\omega_p}{\omega} \right)^2 \quad Y = \frac{\omega_c}{\omega} \quad \rho = \text{LO mode : 1, RX mode : -1}$$

\vec{r}, t : position of a ray path and time

θ : an angle between wave normal vector and the local magnetic field vector

ω_p : plasma frequency (depending on plasma density)

ω_c : cyclotron frequency (depending on magnetic field)

3-2. Ganymede ionosphere result

Focus on ingress

No refraction

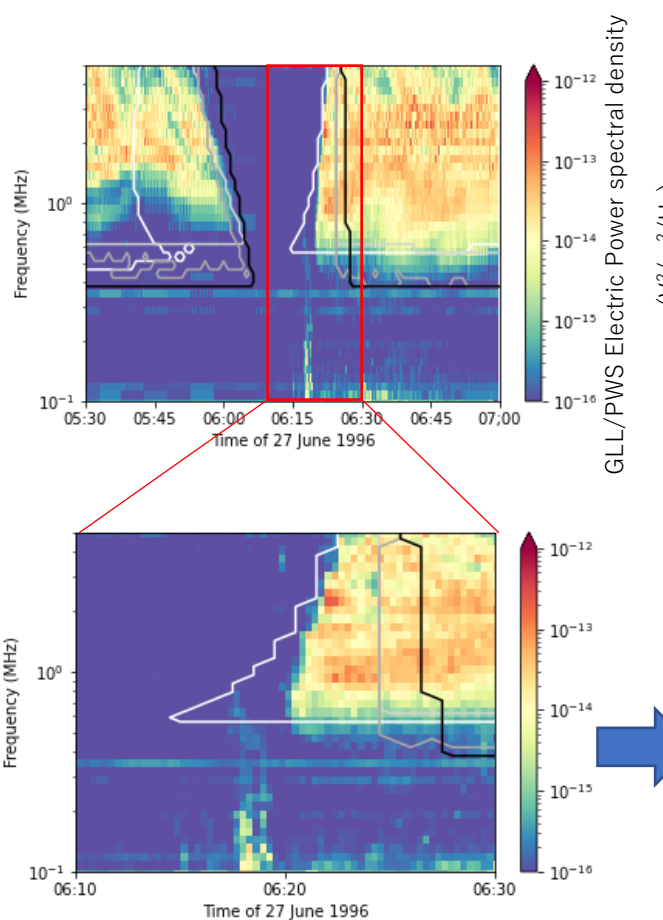


Fig.16 Superimposed Galileo PWS data and ExPRES simulations during Jovian radio emission occultations' egress by Ganymede . The four types of emission (A, B, C, D) are separated (from white to darkgrey, resp.)

Refraction

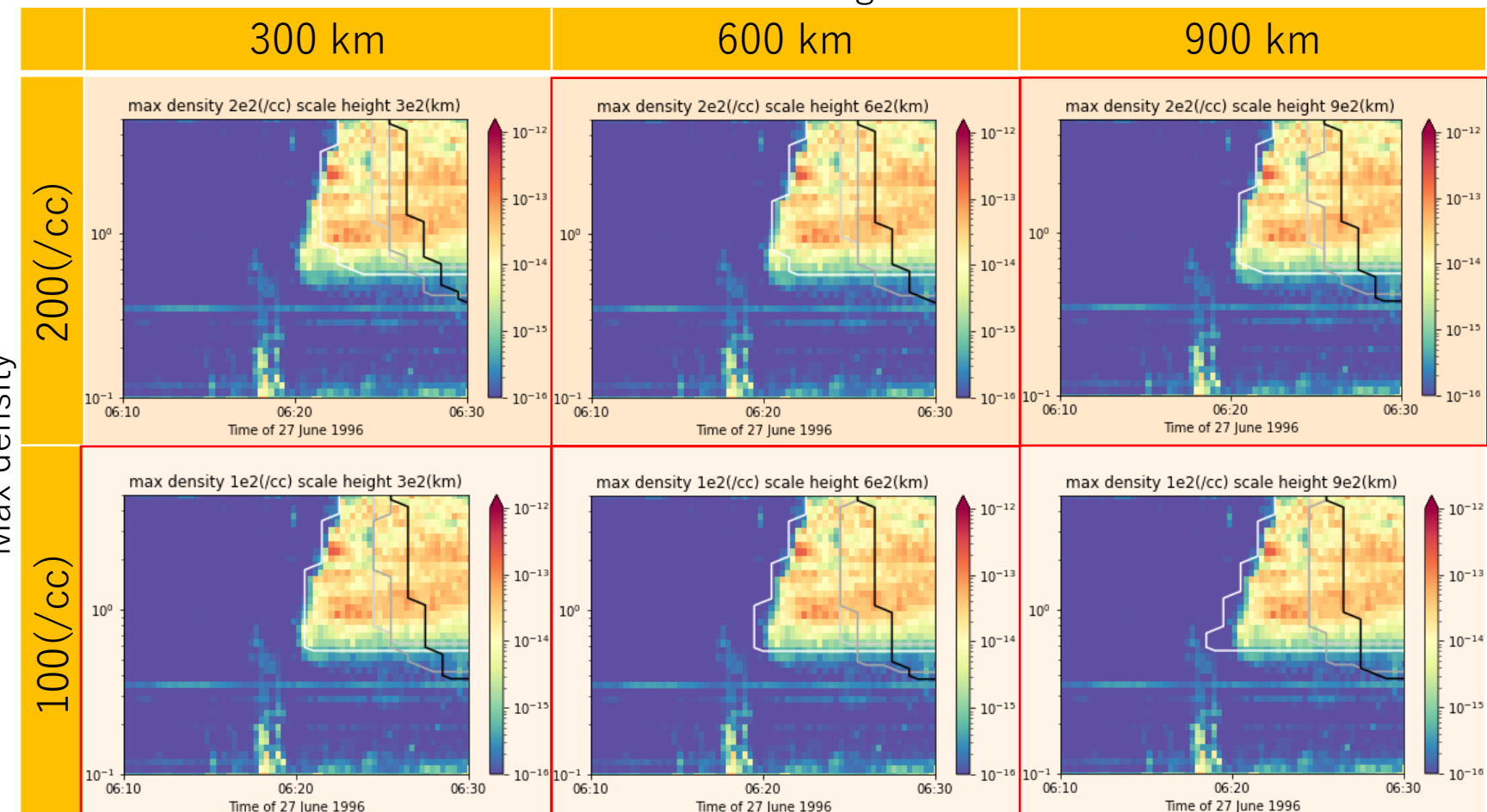


Fig.17 Superimposed Galileo PWS data and our results, assuming hydrostatic equilibrium plasma
[Max density : 200 • 100 (/cc) Scale height : 300 • 150 (km)]

3-2. Ganymede ionosphere result

Focus on egress

No refraction

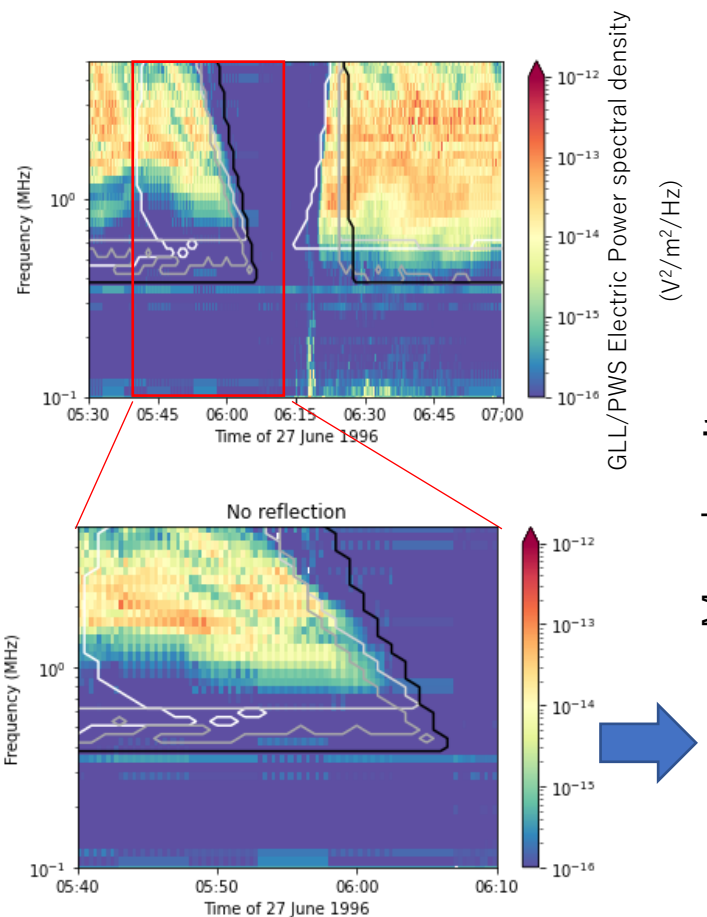


Fig.18 Superimposed Galileo PWS data and ExPRES simulations during Jovian radio emission occultations' egress by Ganymede . The four types of emission (A, B, C, D) are separated (from white to darkgrey, resp.)

Refraction

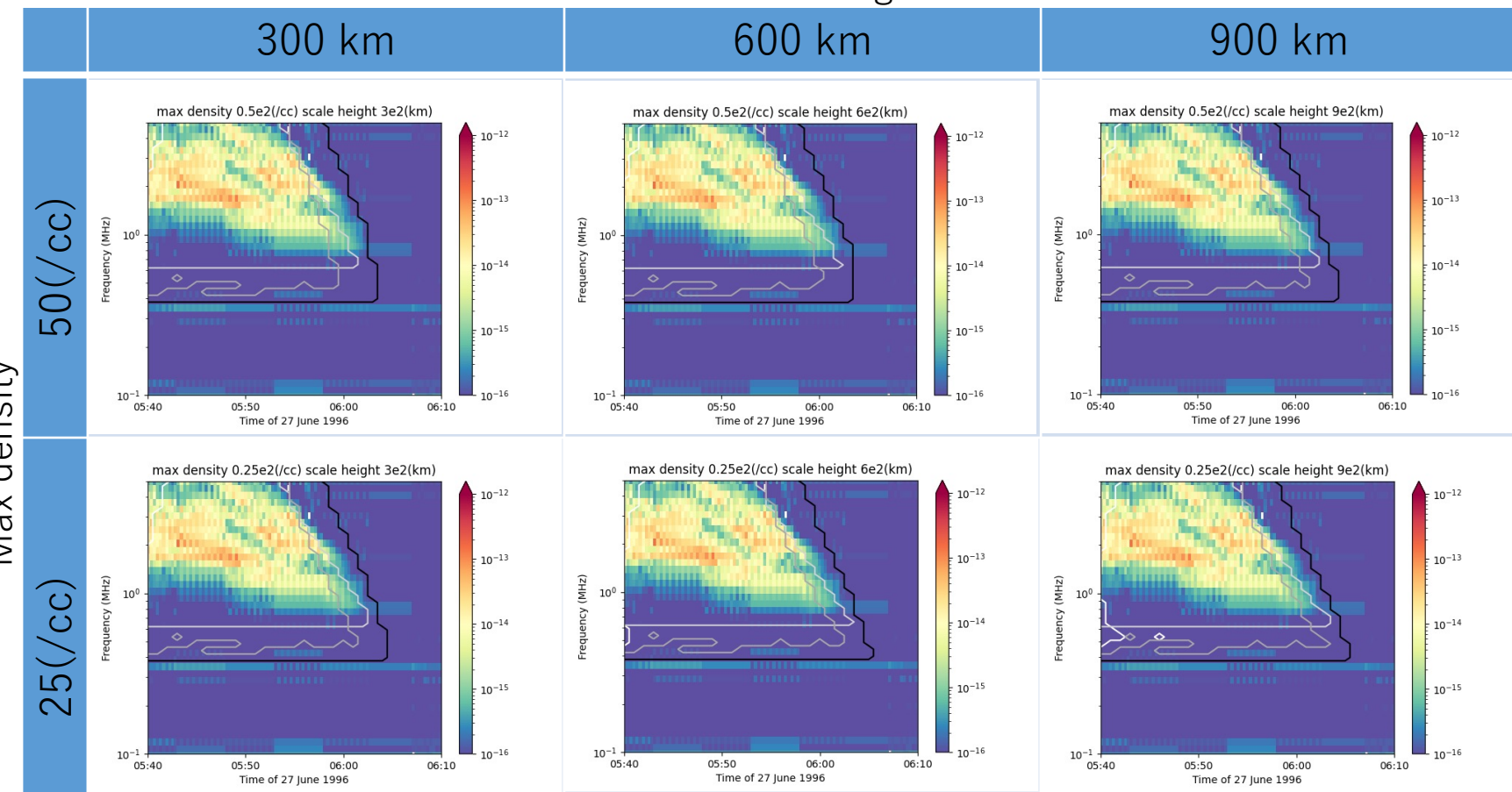


Fig.19 Superimposed Galileo PWS data and our results, assuming hydrostatic equilibrium plasma
[Max density : 50 · 25 (/cc) Scale height : 300 · 150 (km)]

To discuss more quantitatively ...

1. Check radio intensity and the number.
2. Make histogram of the intensity. (Fig. 20)
3. Determine the threshold value [$10e-15(V^2 / m^2 / Hz)$]
4. Determine ingress and egress timings.
5. Calculate average of the difference between the timing and our simulation result for each frequency.

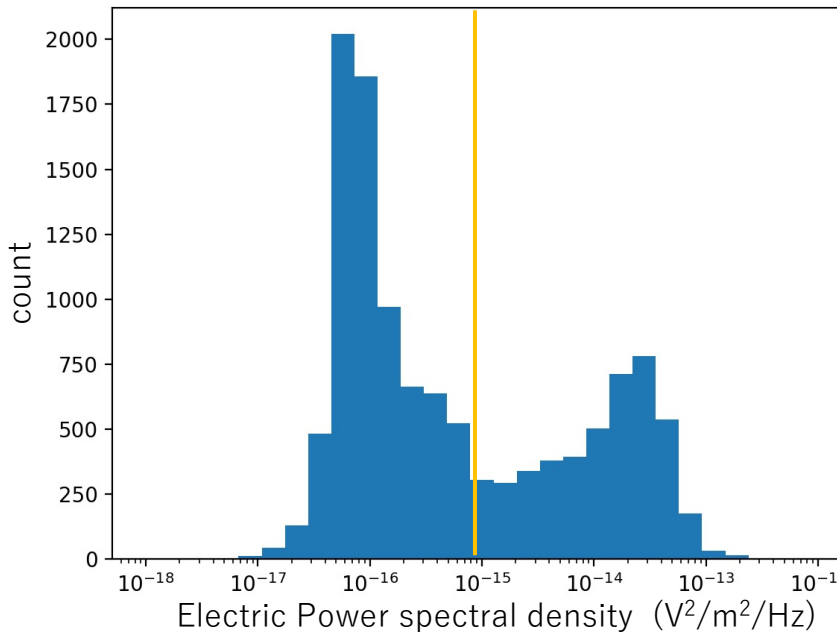


Fig.20 Histogram of the Galileo PWS data intensity

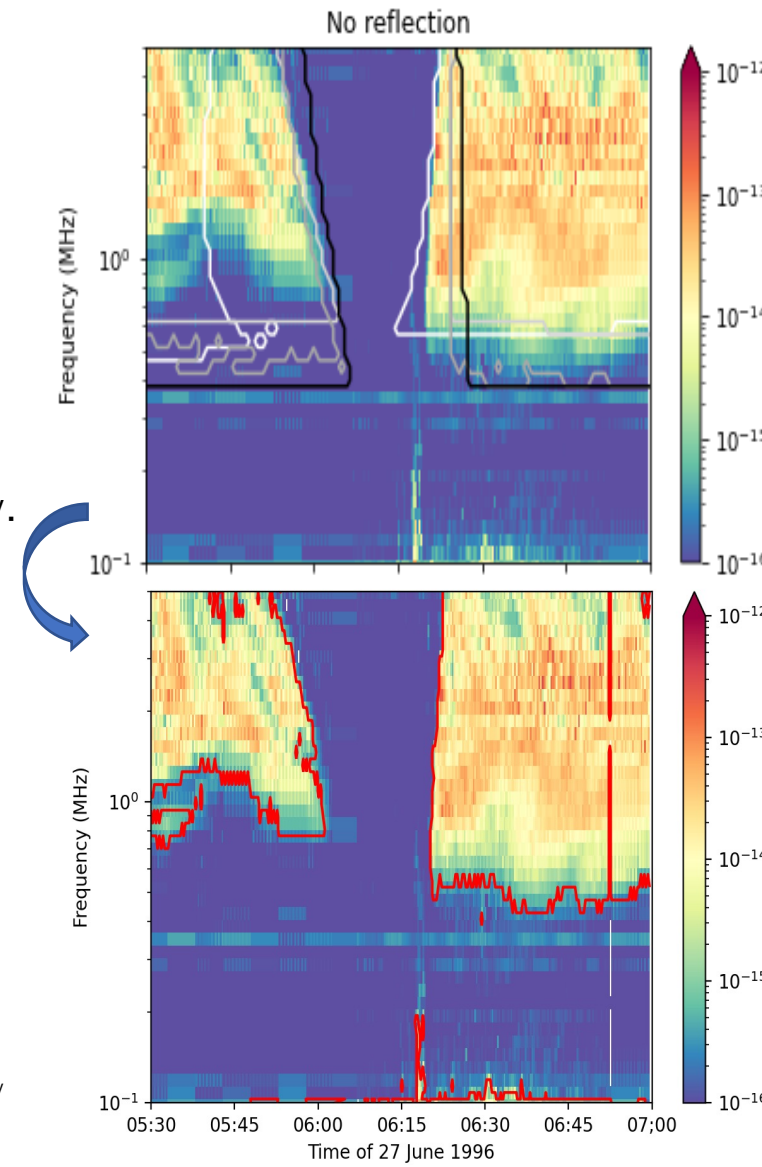


Fig.10 Superimposed Galileo PWS data and ExPRES simulations during Jovian radio emission occultations by Ganymede . The four types of emission (A, B, C, D) are separated (from white to darkgrey, resp.) [Cecconi et al, 2021]

Fig.21 Superimposed Galileo PWS data and boundary between detectable radio and ingress and egress timings.

Focus on ingress

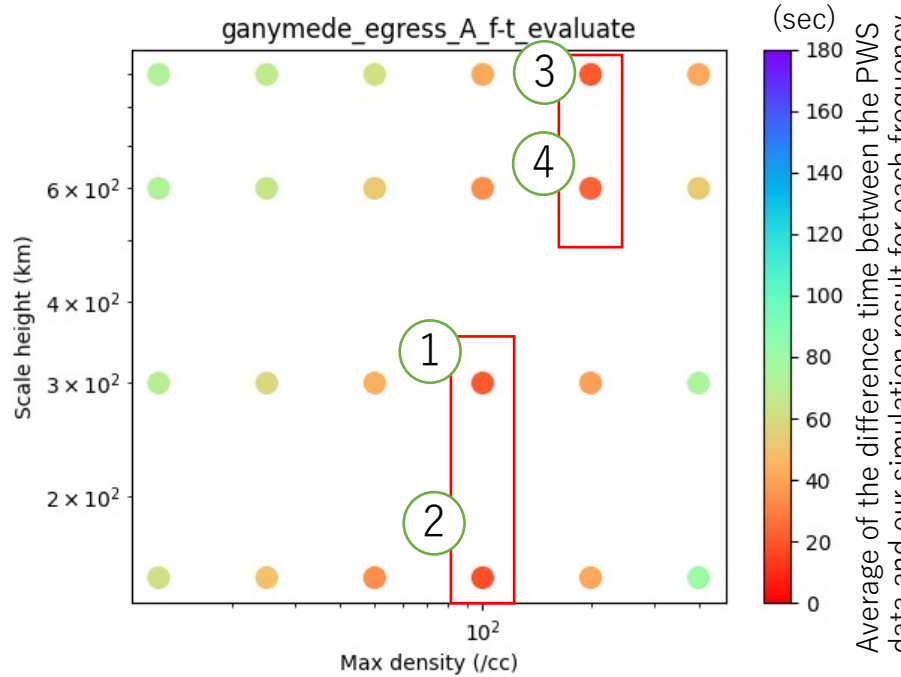


Fig.22 Average of the difference between ingress timing and our simulation result for each frequency, assumed max density and scale height of ionosphere distribution

Electron density distribution

- Scale height 150 (km) - Max 100 (/cc)
- Scale height 300 (km) - Max 100 (/cc)
- Scale height 600 (km) - Max 200 (/cc)
- Scale height 900 (km) - Max 200 (/cc)

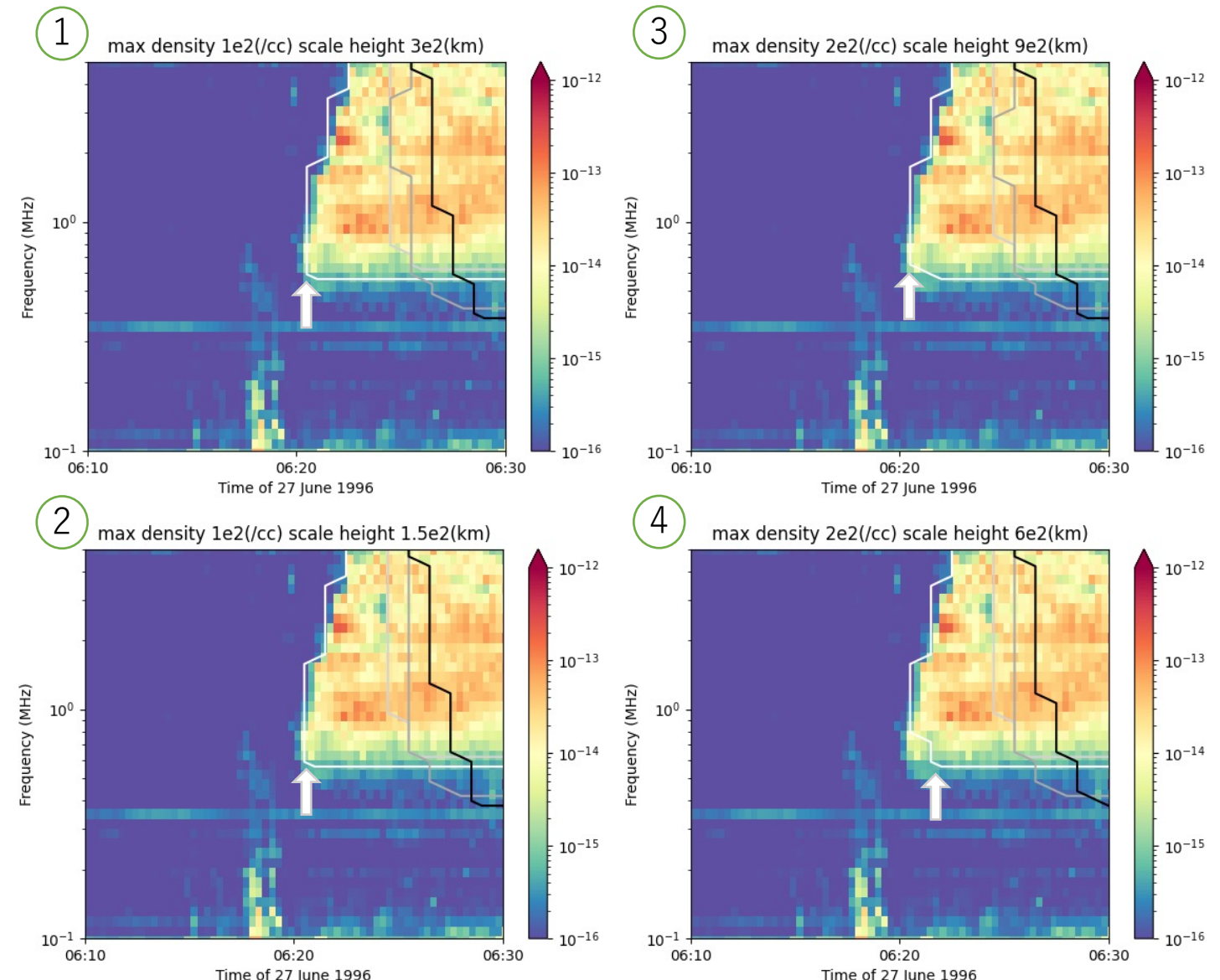


Fig.23 Superimposed Galileo PWS data and our results, assuming hydrostatic equilibrium plasma
[Max density and Scale height : 100 (/cc) & 300 (km) / 100 (/cc) & 150 (km) / 200 (/cc) & 900 (km) / 200 (/cc) & 600 (km)]

3-3. Discussion

26

Focus on egress

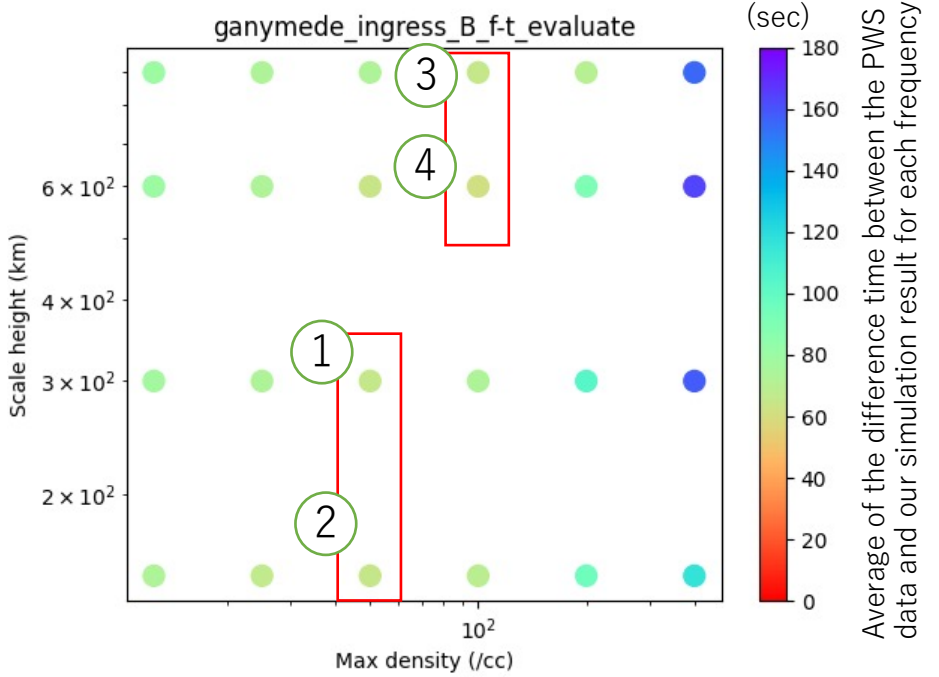


Fig.24 Average of the difference between egress timing and our simulation result for each frequency, assumed max density and scale height of ionosphere distribution

Electron density distribution

- Scale height 150 (km) - Max 50 (/cc)
- Scale height 300 (km) - Max 50 (/cc)
- Scale height 600 (km) - Max 100 (/cc)
- Scale height 900 (km) - Max 100 (/cc)

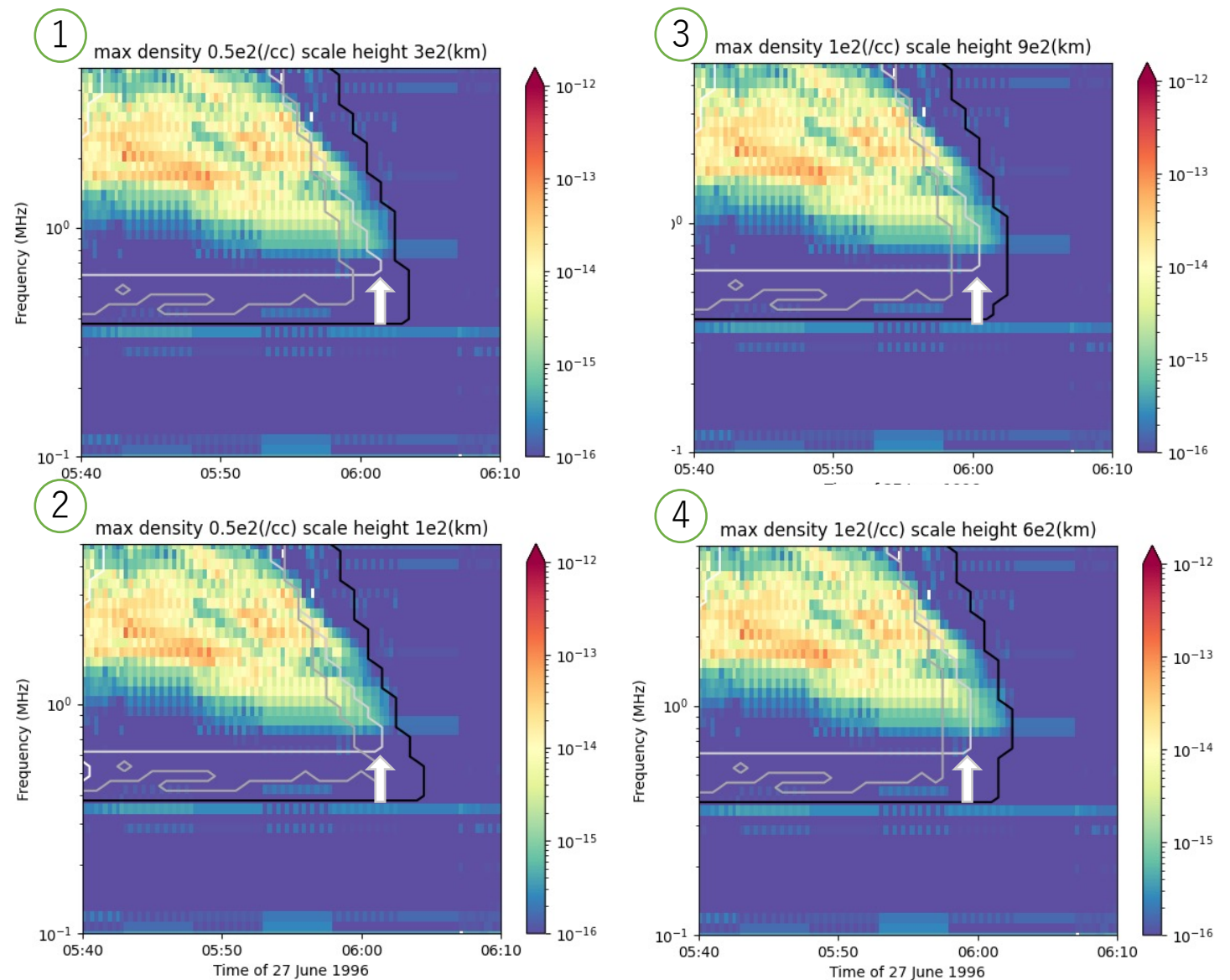


Fig.25 Superimposed Galileo PWS data and our results, assuming hydrostatic equilibrium plasma
[Max density and Scale height : 50 (/cc) & 300 (km) / 50 (/cc) & 100 (km) / 100 (/cc) & 900 (km) / 100 (/cc) & 600 (km)]

In-situ observation [Galileo PWS] and our results

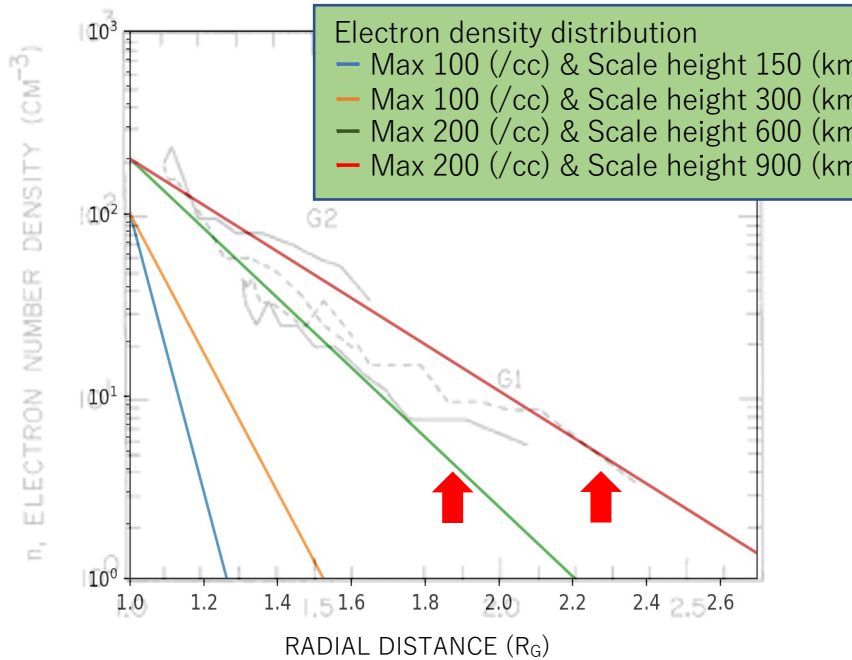


Fig.6 Electron density profiles on Ganymede 2 obtained by means of the PWS instrument on Galileo [Eviatar et al, 2001] and Electron density distribution during Ganymede G1 flyby that we estimate

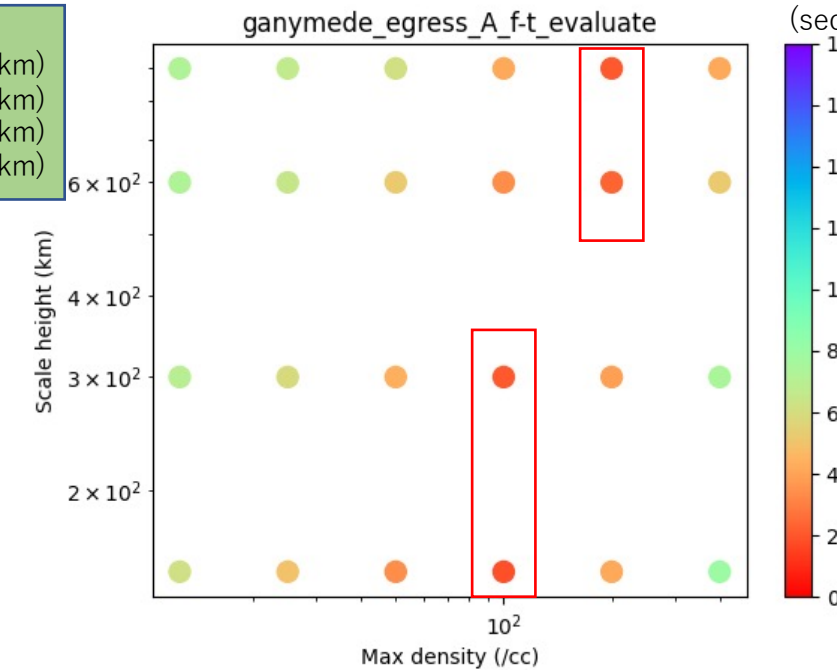
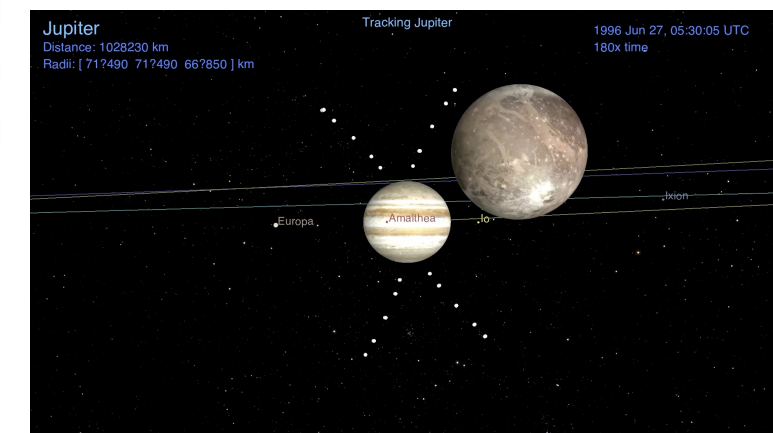


Fig.16 Superimposed Galileo PWS data and ExPRES simulations during Jovian radio emission occultations' egress by Ganymede . The four types of emission (A, B, C, D) are separated (from white to darkgrey, resp.)



- Some of our results (ex. red and green lines in Fig.15) match the In-situ observation results!
- Our results have strong sensitivity to maximum electron density.

In combination with In-situ observation, we can estimate the structure of the ionosphere.

[Background]

- Structures of the interior, ionosphere and plume of the icy moons are essential information for understanding universality of habitable environment.

[Purpose]

- Developing the numerical simulation code for the radar explorations using natural radio waves to investigate spatial structures of ionosphere and plumes created from the water oceanic materials.
- Finally, we will also investigate spatial structures of the interior.

[Result]

- Hydrostatic equilibrium plasma ionosphere model can explain the Galileo PWS data during Jovian radio emission occultations.

[Discussion]

- Some of our results (ex. red and green lines in Fig.15) match the In-situ observation results!
- In combination with In-situ observation, we can estimate the structure of the ionosphere.

~ For occultation ~

- ・ パラメータスタディをもう少しだけ進める（年内）
- ・ この手法を他のガリレオPWSデータに適用・エウロパ&カリストの電子密度推定（年内～1月）
- ・ 惑星電波を用いた電離圏掩蔽観測で論文執筆（年度内）

~ For passive Rader ~

- ・ 指定した確率で氷衛星表面で反射・透過する電波の再現（済）
- ・ 掩蔽論文執筆後、コード開発を再開（M2でのテーマ？）

~ For GPEES and doctoral course~

- ・ パリ天文台の方々に自身の結果を共有（部分的にはメールで共有済み）+この資料を手直して改めて共有・相談
- ・ 博士での大まかな研究テーマ共有（12月上旬）
- ・ テーマ案 …・東北大コードとExPRESの組み合わせた掩蔽&レーダー観測手法の確立（設計次第）
- ・ GPEES願書作成（12月上旬）&提出（1月上旬）

1-2. Ionosphere of Jupiter's icy moon

30

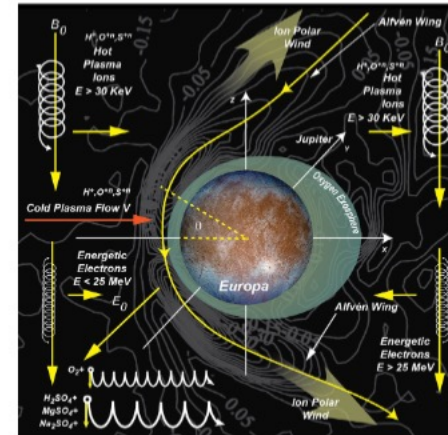
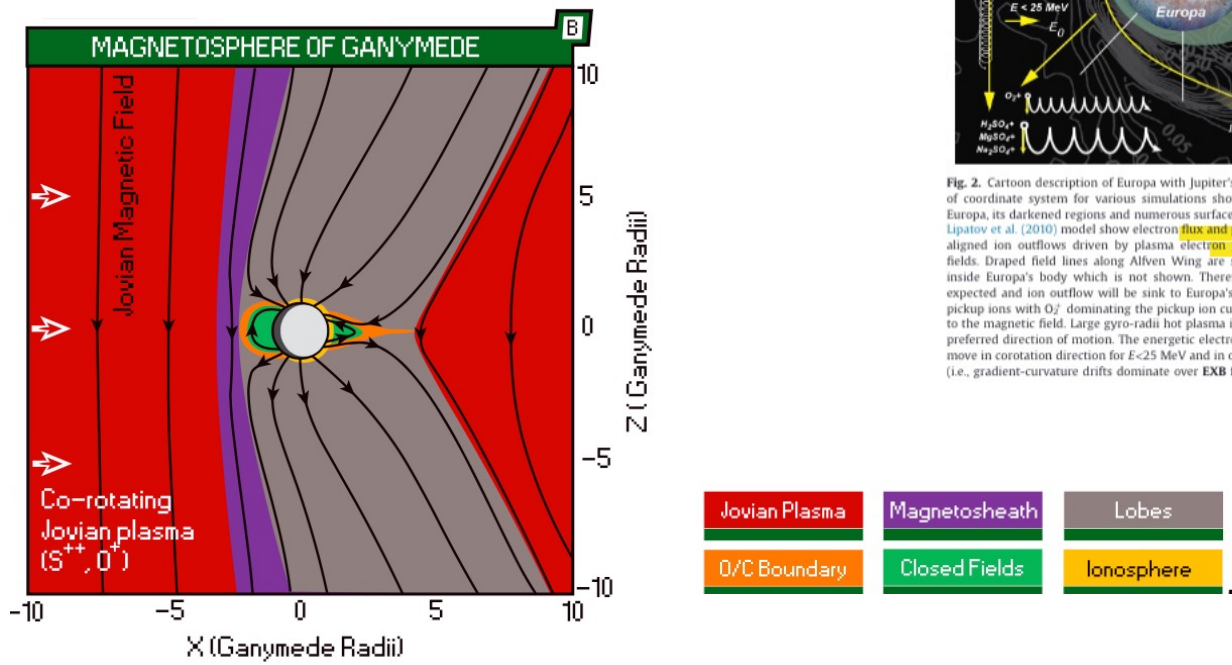


Fig. 2. Cartoon description of Europa with Jupiter's magnetosphere and definition of coordinate system for various simulations shown. It shows surface image of Europa, its darkened regions and numerous surface cracks. Intensity contours from Lipatov et al. (2010) model show electron flux and possible presence of polar field-aligned ion outflows driven by plasma electron produced field aligned electric fields. Draped field lines along Alfvén Wing are shown. Field lines then diffuse inside Europa's body which is not shown. Therefore, field aligned currents are expected and ion outflow will be sink to Europa's ionosphere. Figure also shows pickup ions with O₂⁺ dominating the pickup ion current which flow perpendicular to the magnetic field. Large gyro-radius hot plasma ions are shown along with their preferred direction of motion. The energetic electrons have smaller gyro-radii and move in corotation direction for $E < 25$ MeV and in opposite direction for $E > 25$ MeV (i.e., gradient-curvature drifts dominate over EXB flow).

Observation	Lat (deg)	W. Long	SZA	Ram Angle
Europa 4 entry	-2	346	95	76
Europa 4 exit	-4	167	85	103
Europa 6a entry	-24	281	86	11
Europa 6a exit	-21	102	94	168
Europa 6b entry	-14	56	85	146
Europa 6b exit	-14	236	85	34

Fig. Geometry of Galileo occupations by Europa.

Ganymede ionosphere

In-situ observation of Galileo flyby [Galileo plasma-wave instrument] (Fig.6)

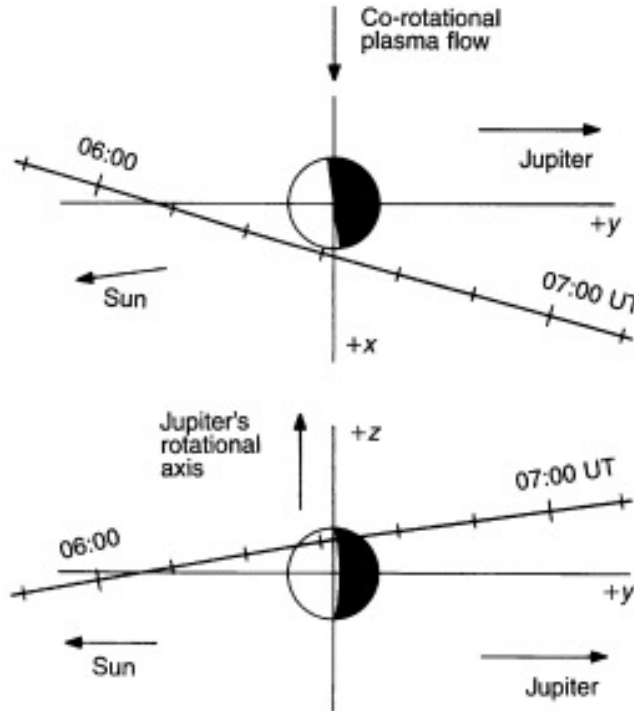


FIG. 1 The trajectory of Galileo during the first Ganymede fly-by. The Ganymede-centred coordinate system has the $+z$ axis aligned parallel to Jupiter's rotational axis and the $+x$ axis parallel to the nominal co-rotational plasma flow induced by Jupiter's rotation. The top diagram shows the view looking towards the $+z$ axis, and the bottom diagram shows the view looking towards the $+x$ axis.

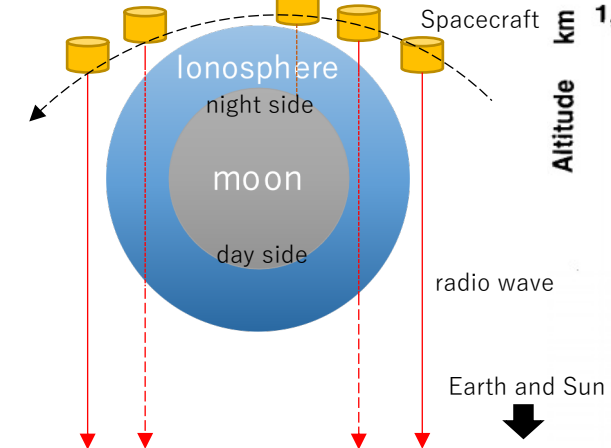
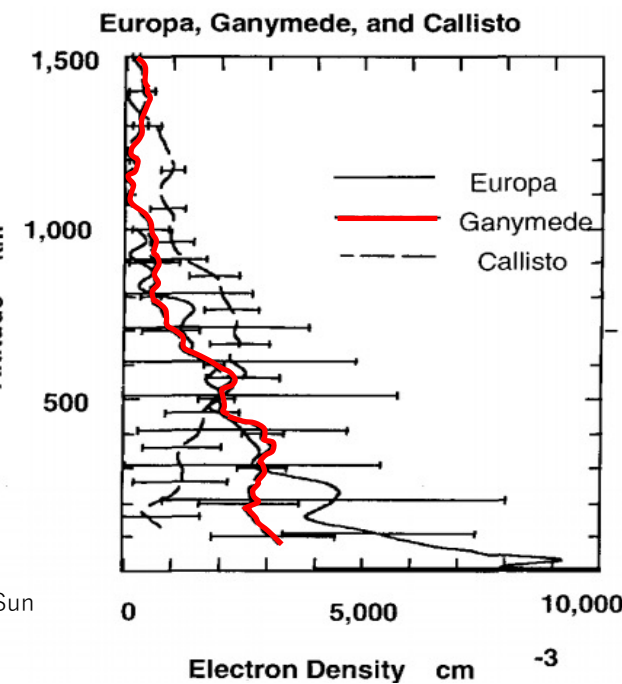


Fig.7 Radio observation using Jovian radio ref



Appleton-Hartree equation

~The dispersion relation of waves in magnetized cold plasma~

$$D(t, \vec{r}, \omega, \vec{k}) = \left(\frac{c|\vec{k}|}{\omega}\right)^2 + \frac{2X}{2 - \frac{Y^2 \sin^2 \theta}{1-X} + \rho \sqrt{\frac{Y^2 \sin^4 \theta}{(1-X)^2} + 4Y^2 \cos^2 \theta}} - 1 = 0 \quad \cdots (1)$$

$$X = \left(\frac{\omega_p}{\omega}\right)^2 \quad Y = \frac{\omega_c}{\omega} \quad \rho = \begin{cases} 1 & \text{LO mode} \\ -1 & \text{RX mode} \end{cases}$$

\vec{r}, t : position of a ray path and time

θ : an angle between wave normal vector and the local magnetic field vector

ω_p : plasma frequency (depending on plasma density)

ω_c : cyclotron frequency (depending on magnetic field)

- Derived from the equation of motion for plasma and Maxwell's equation
(Cold plasma · Discarding plasma collision)

- Under the Eq-(1) condition, electromagnetic wave in plasma can exist.
- Trace the ray propagation meeting this condition.

... Raytracing

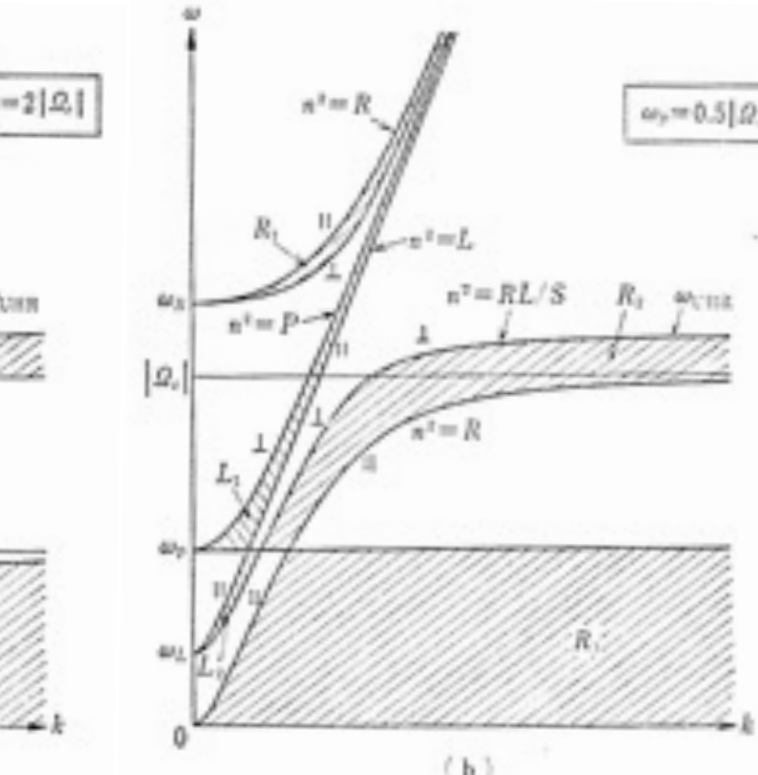
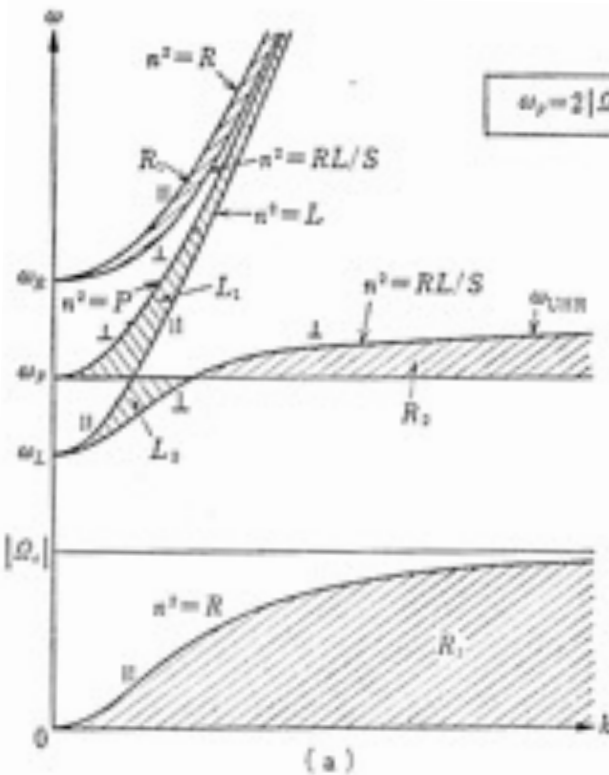


Fig.16 $\omega - k$ diagram ($\omega_p = 2|\Omega_e|, \omega_p = 0.5|\Omega_e|$) ["Gendai Denjihadouron"]

[Hess et al., 2008]

ExPRES code

- ・観測者的位置に伝わってくる電波が時間ごとにどのようなスペクトルをもつかモデリングするシミュレーションコード

～フリーパラメータ～

- ・ある時刻における観測者・イオ・木星の位置関係
- ・リード角 δ …電波源となる磁力線とイオを貫く磁力線の経度差
- ・磁場モデル
- ・電子の速度分布の種類→ビーム角 θ の指定
 - …ロスコーンタイプの場合 40-80° 程度
ロスコーン角の大きさで決定
 - …シェルタイプの場合 90°(const)付近
- ・ビーム角の厚み $\delta\theta$

(直進波を仮定)

時間ごとに観測される周波数を
周波数 - 時間平面で表示

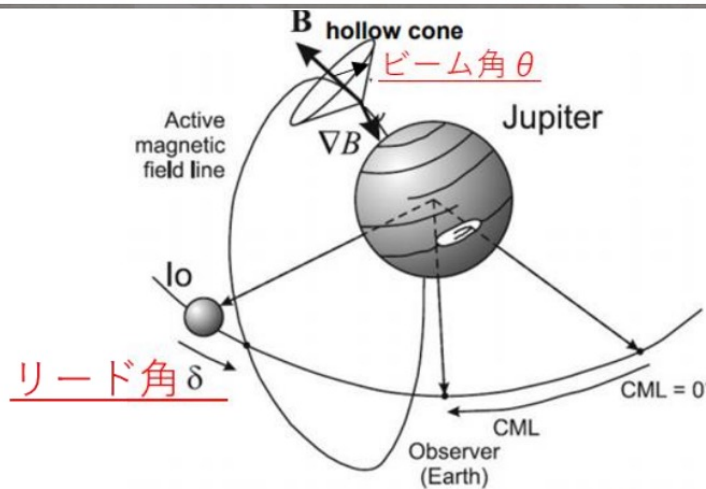


Fig.18 パラメータの位置関係 [Galopeau et al. 2007]

電波源との位置関係
と周波数が決定

電波放射の
向きと幅が決定

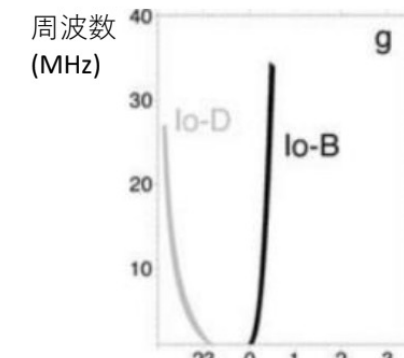


Fig.19 シミュレーション結果の一例 [Hess et al., 2008]

CMI (サイクロトロンメーザー不安定)

- ①磁力線周りに旋回しながら伝搬する電波と電子が同じ周期
(もしくはその整数倍で) で振動する (共鳴条件)
- ②プラズマ物理の理論から計算される電波の成長率が有意に大きい

①と②の条件により

→電子の磁力線水平・垂直方向の速度に対する分布「速度分布関数」の形状によって
成長率が最大となるビーム角 θ が定まる

電波の成長を引き起こす代表的な二つの速度分布関数の有力候補

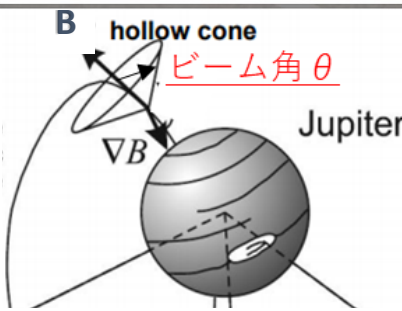
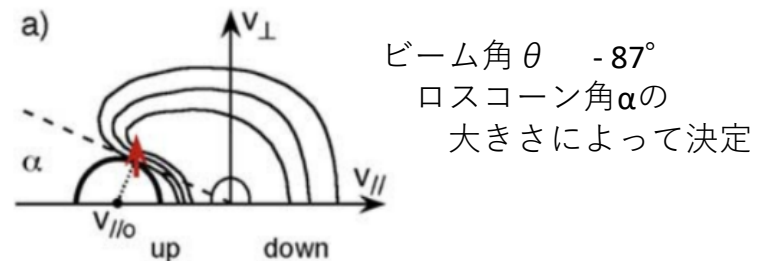


Fig.18 パラメータの位置関係
[Galopeau et al. 2007]

a) 口スコーンタイプ
‥電子の全方向へのランダムな加速



b) シェルタイプ
‥電子の v_{\parallel} 方向のモノリシックな加速

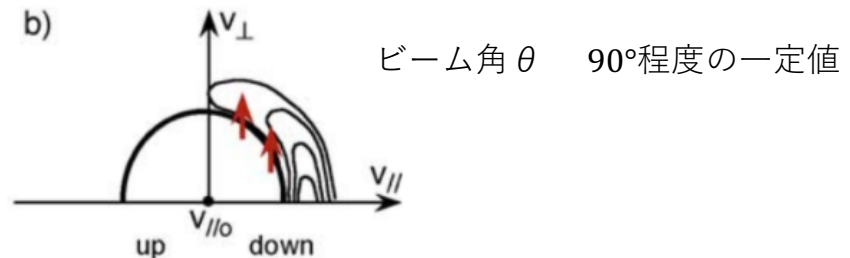


Fig.19 各タイプの電子の速度分布関数[Hess et al., 2008]

測度分布関数の解明 → 加速過程の解明

木星探査機Juno/Waves による波動観測結果との比較 [Louis et al., 2017]

- ・モデルとの比較による観測された電波源の位置（北or南半球）の識別
- ・Junoの周回衛星ならではの広い緯度域からの新たにパラメータの制約が可能に
→より正確にCMIによる電波放射の観測を再現するシミュレーションに成功
→電子・イオンの直接観測と比較

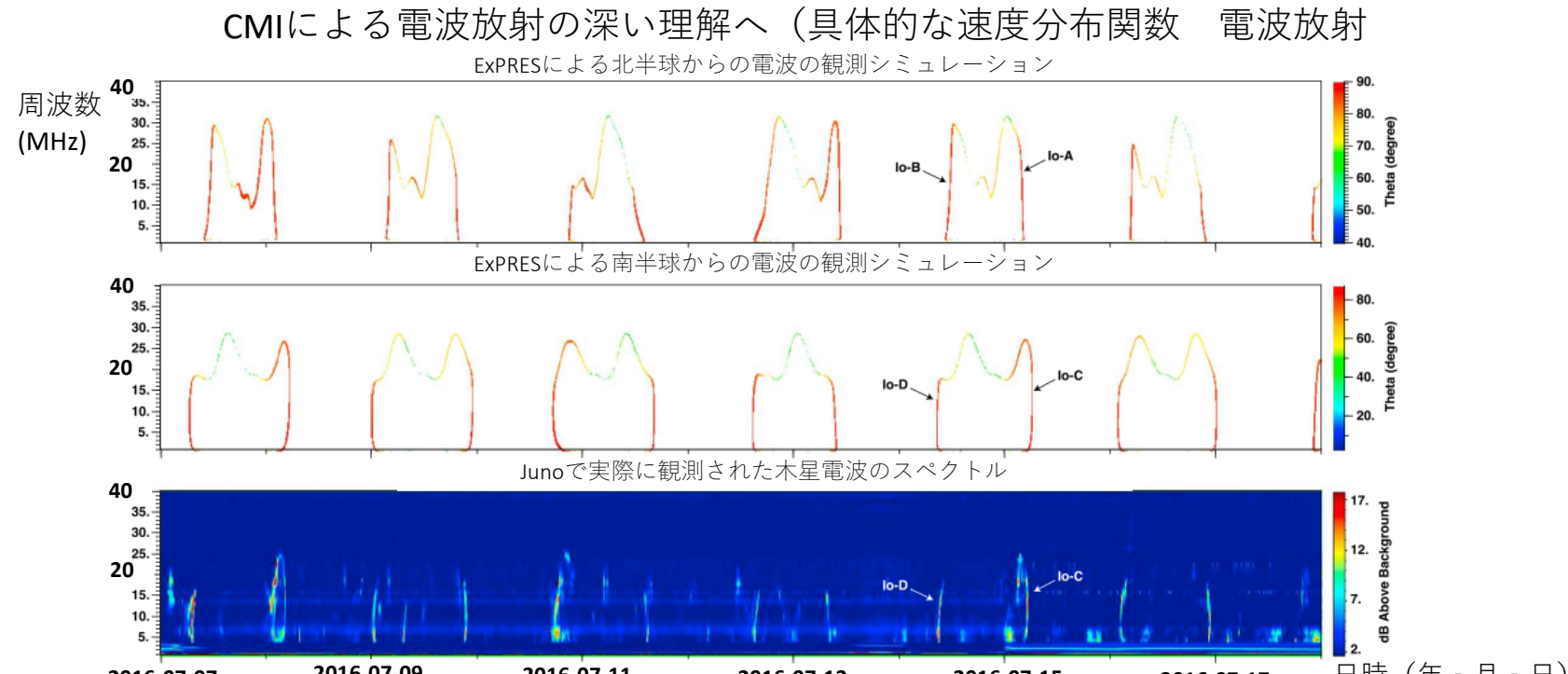


Fig.20 下から Junoで観測された木星電波のスペクトル、ExPRESによる南半球からの電波の観測シミュレーション
ExPRESによる北半球からの電波の観測シミュレーション [Louis et al., 2017a]

速度分布関数のタイプから発生する放射角の導出方法

- ①伝搬している電波と電子が同じ周期（もしくはその整数倍で）で振動する（共鳴条件）

$$\text{共鳴条件} \cdots \omega = \frac{\omega_{CE}}{\Gamma} + k_{\parallel} v_{\parallel}$$

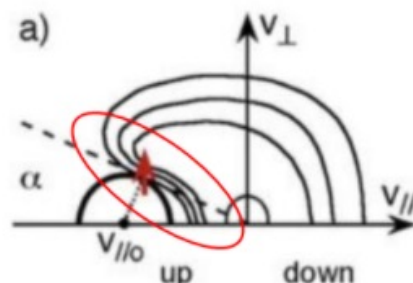
$\rightarrow v_{\parallel 0} \sim c \cos \theta$ を中心とした速度平面上の円にある電子が電波法射

- ②プラズマ物理の理論から計算される共鳴による電波の成長率が有意に大きい

$$\text{電波の成長率} \cdots \gamma \propto \int_{R.C.} v_{\perp}^2 \nabla v_{\perp} f(v) dv \quad (\text{積分経路} \cdots \text{共鳴条件の速度平面上の円})$$

$\rightarrow \nabla v_{\perp} f(v) > 0$ となるような積分経路を持つ円での放射大

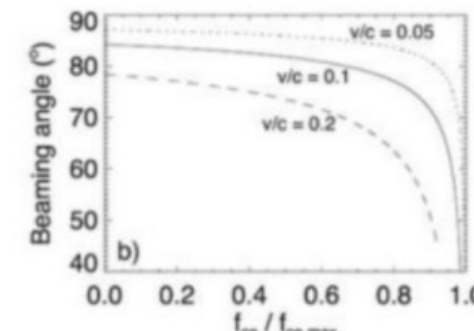
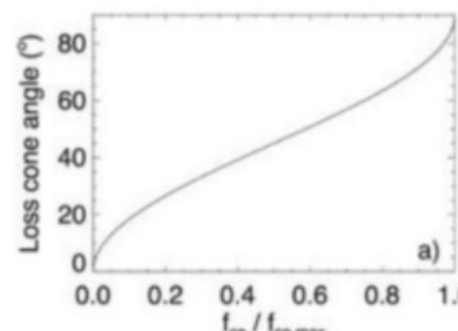
a) ロスコーンタイプ



$$v_{\parallel 0} = v / \cos \alpha = v / \left(1 - \frac{\omega_{ce}}{\omega_{ce,max}} \right)^{1/2}$$

$$\rightarrow \theta = \arccos \left[(v/c) / \left(1 - \omega_{ce} / \omega_{ce,max} \right)^{1/2} \right]$$

ビーム角 θ 鋭角(40-80° 程度)
ロスコーン角 α の大きさで決定



JUICE RPWI – HF – RWI preamp : Required Spec.s

- Developed by Tohoku Univ.(Jpn), Meisei Elec.(Jpn) & Astronika (Pol) since 2010
- Required specifications:

Item	Required spec.	Comments
Frequency	80KHz ~ 45MHz	Fully covering Jupiter's LF – HF radio emissions (KOM – DAM)
Temperature	-180 ~ +100degC (storage) > -150degC* (operation)	Ganymede (shade) ~ Venus orbit *on PCB
Radiation dose	100krad with t=10mm Al (operation)	in Jupiter's inner magnetosphere
Gain	> 10dB	Compensation of connection loss between Antenna and RWI keeping low noise level
Noise level	< 4×10^{-20} W/m ² /Hz (4nV/m/ $\sqrt{\text{Hz}}$) @1MHz → <10nV/ $\sqrt{\text{Hz}}$ @L=2.5m	Below Galactic noise @1MHz
Dynamic range	5μV/m/ $\sqrt{\text{Hz}}$ ~ 4nV/m/ $\sqrt{\text{Hz}}$ → >52dB	Fully covering Jupiter's LF – HF radio emissions (KOM – DAM) on Jupiter's orbit (Max. signal level is near Europa.)
Ch–Ch Phase diff.	(<1deg)	On-flight calibration will be made.
Power consumption	~430mW (w/o heater) ~800mW (with heater)	Requirement from power-management

Ray tracing [Kimura et al, 2008a, b, 2010 etc..] (Cf. Appendix G&H)

~ input parameter ~

- Magnetic field model $\omega_c(\vec{r}, t)$
- Plasma density model $\omega_p(\vec{r}, t)$
- Frequency of wave (ω)
- Initial position (\vec{r}_0)
- Initial wave vector (\vec{k}_0)



$d\vec{r}_{j+1}$ and $d\vec{k}_{j+1}$ in dt_j

$$(1) \rightarrow d\vec{r}_{j+1} = -\frac{\partial D_j / \partial \vec{k}_j}{\partial D_j / \partial \omega} \cdot dt_j, \quad d\vec{k}_{j+1} = +\frac{\partial D_j / \partial \vec{r}_j}{\partial D_j / \partial \omega} \cdot dt_j$$



the time (t_{j+1}), position (\vec{r}_{j+1}) and wave vector (\vec{k}_{j+1}) after dt_j

- $t_{j+1} = t_j + dt_j$
- $\vec{r}_{j+1} = \vec{r}_j + d\vec{r}_{j+1}$
- $\vec{k}_{j+1} = \vec{k}_j + d\vec{k}_{j+1}$



~ output ~

a full ray path and time ($\vec{r}(t)$)

• Equation of motion of plasma

$$\frac{d\vec{v}}{dx} = \frac{q}{m} (\vec{E} + \vec{v} \times \vec{B})$$

• Maxwell's equations

$$\nabla \times \vec{H} = \vec{j} + \frac{\partial \vec{D}}{\partial t} \quad \nabla \times \vec{E} = -\frac{\partial \vec{B}}{\partial t}$$



(Cold plasma • Discarding plasma collision)

Appleton-Hartree equation (Cf. Appendix A)

~The dispersion relation of waves in magnetized cold plasma~

$$D(t, \vec{r}, \omega, \vec{k}) = \left(\frac{c|\vec{k}|}{\omega} \right)^2 + \frac{2X}{2 - \frac{Y^2 \sin^2 \theta}{1-X} + \rho \sqrt{\frac{Y^2 \sin^4 \theta}{(1-X)^2} + 4Y^2 \cos^2 \theta}} - 1 = 0 \quad \dots (1)$$

$$X = \left(\frac{\omega_p}{\omega} \right)^2 \quad Y = \frac{\omega_c}{\omega} \quad \rho = \text{LO mode : 1, RX mode : -1}$$

\vec{r}, t : position of a ray path and time

θ : an angle between wave normal vector and the local magnetic field vector

ω_p : plasma frequency (depending on plasma density)

ω_c : cyclotron frequency (depending on magnetic field)

Martyn's theorem ~Electromagnetic wave theory ~

- Derived from Snell's law
under plane-stratified electron density distribution

Actual angle of incidence θ_1



Angle of incidence calculated from plasma density and position of reflection point

$$\theta_2 = \tan^{-1} \left(\frac{\int 1/\sqrt{1 - \omega_p(z)^2/\omega_{\perp}^2} dz}{x} \right)$$

Integral range ... incident height ~ reflect height(h)
 $\omega_{\perp} = \omega \cos \theta_1$ (θ_1 ... angle of incidence)

$$d\vec{r}_{j+1} = - \frac{\partial D_j / \partial \vec{k}_j}{\partial D_j / \partial \omega} \cdot dt_j, \quad d\vec{k}_{j+1} = + \frac{\partial D_j / \partial \vec{r}_j}{\partial D_j / \partial \omega} \cdot dt_j$$

1. Calculate θ_2 from the results of ray tracing
2. Compare θ_2 from θ_1

When the results of ray tracing is valid

$$\dots \theta_1 = \theta_2$$

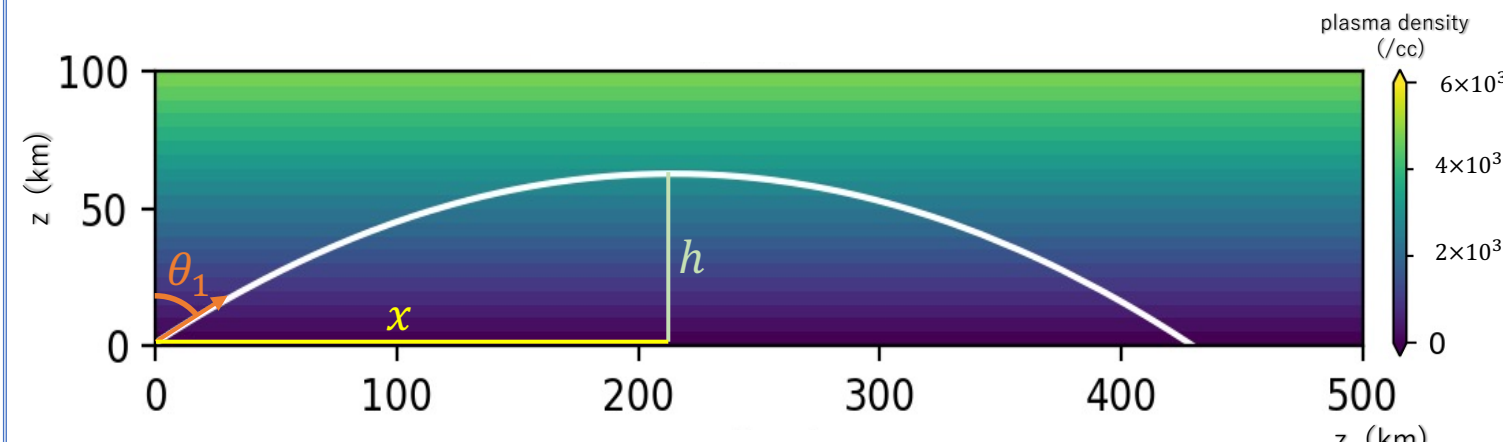


Fig.15 Ray tracing result to verify raytracing-code validity

Plasma density model ... $0.5 \times 10^2 \times [z(\text{km})] (\text{/cc})$

Magnetic field model ... near zero magnetic field ($1.0 \times 10^{-11} (\text{T})$ · The X-axis direction)

Initial wave ... $z = 1 \text{ km}$ · $\theta_1 = 60^\circ$ · LO-mode · 1MHz

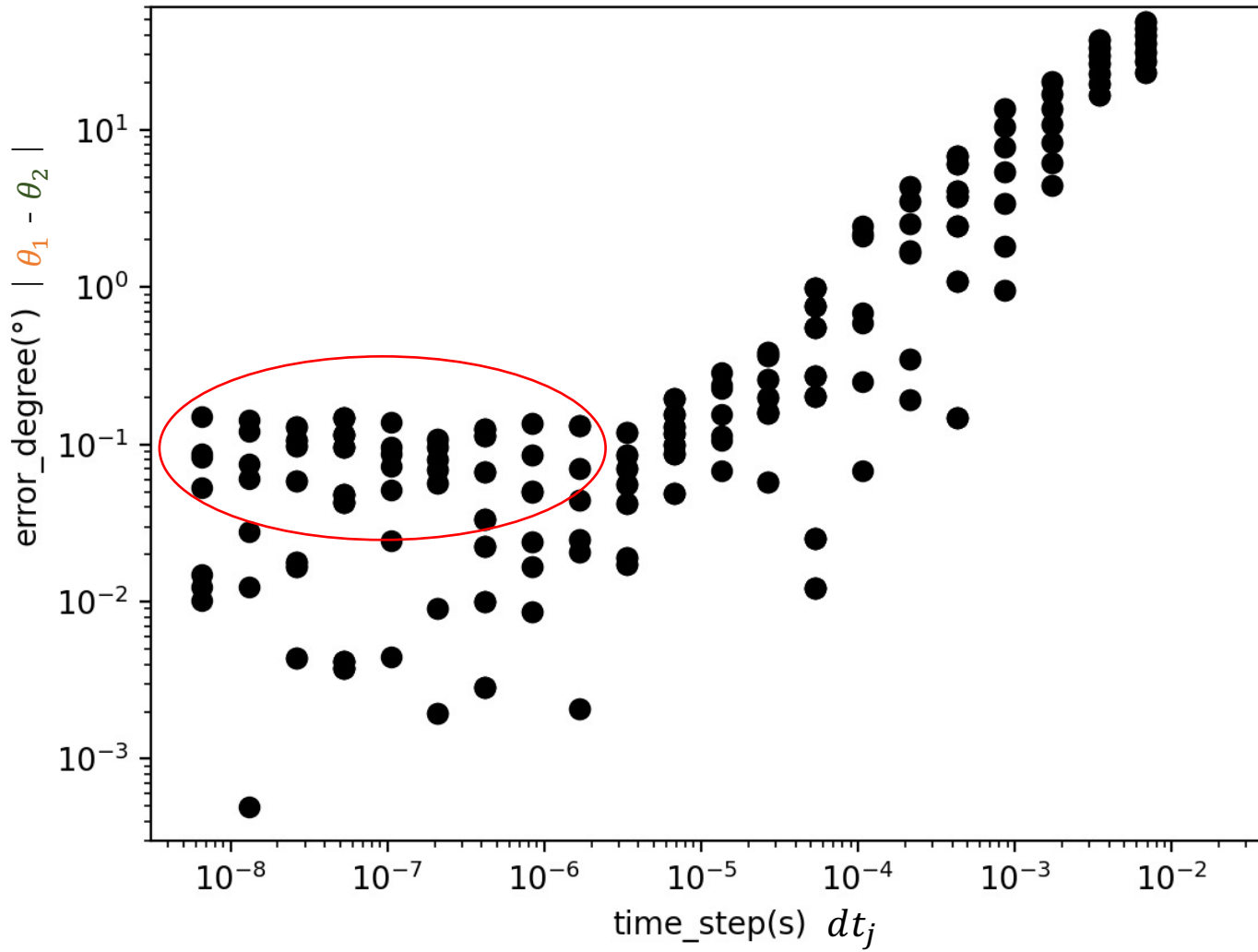


Fig.16 Verify time-step validity of raytracing code

The vertical line

… validity index (| $\theta_1 - \theta_2$ |)

High value → Large calculation error

Low value → Small calculation error

The horizontal line

… time step (dt_j)

→ We need to run this raytracing code
on $\sim 10^{-6}$ (sec) time step.

We validated results of raytracing code and
verified appropriate time step.

- In numerical radar simulation, full wave simulation is general method.

ex) FDTD (Finite-difference time-domain method) method (Fig.13) Δz
 ...Solving Maxwell's equations on a mesh and computing E and H
 at grid points spaced Δx , Δy , and Δz apart.

- However, this method needs high calculation cost when we execute the program in a wide calculation space such as ionosphere, plumes and interiors of icy moons.

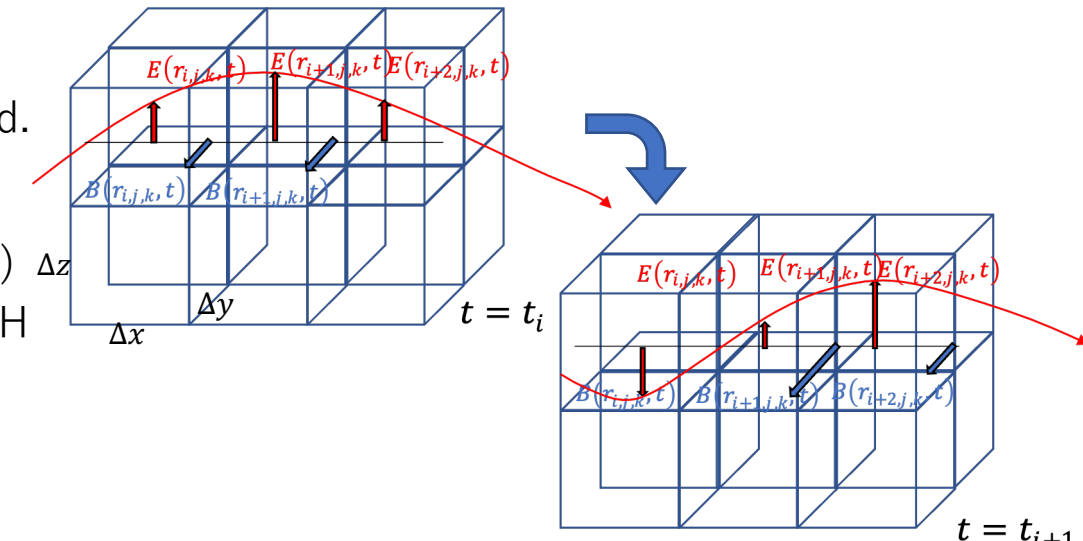


Fig.6 FTDT image

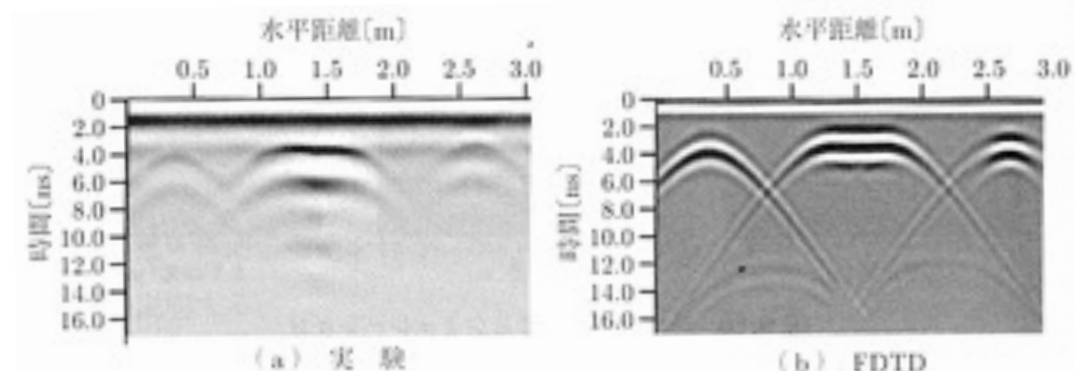
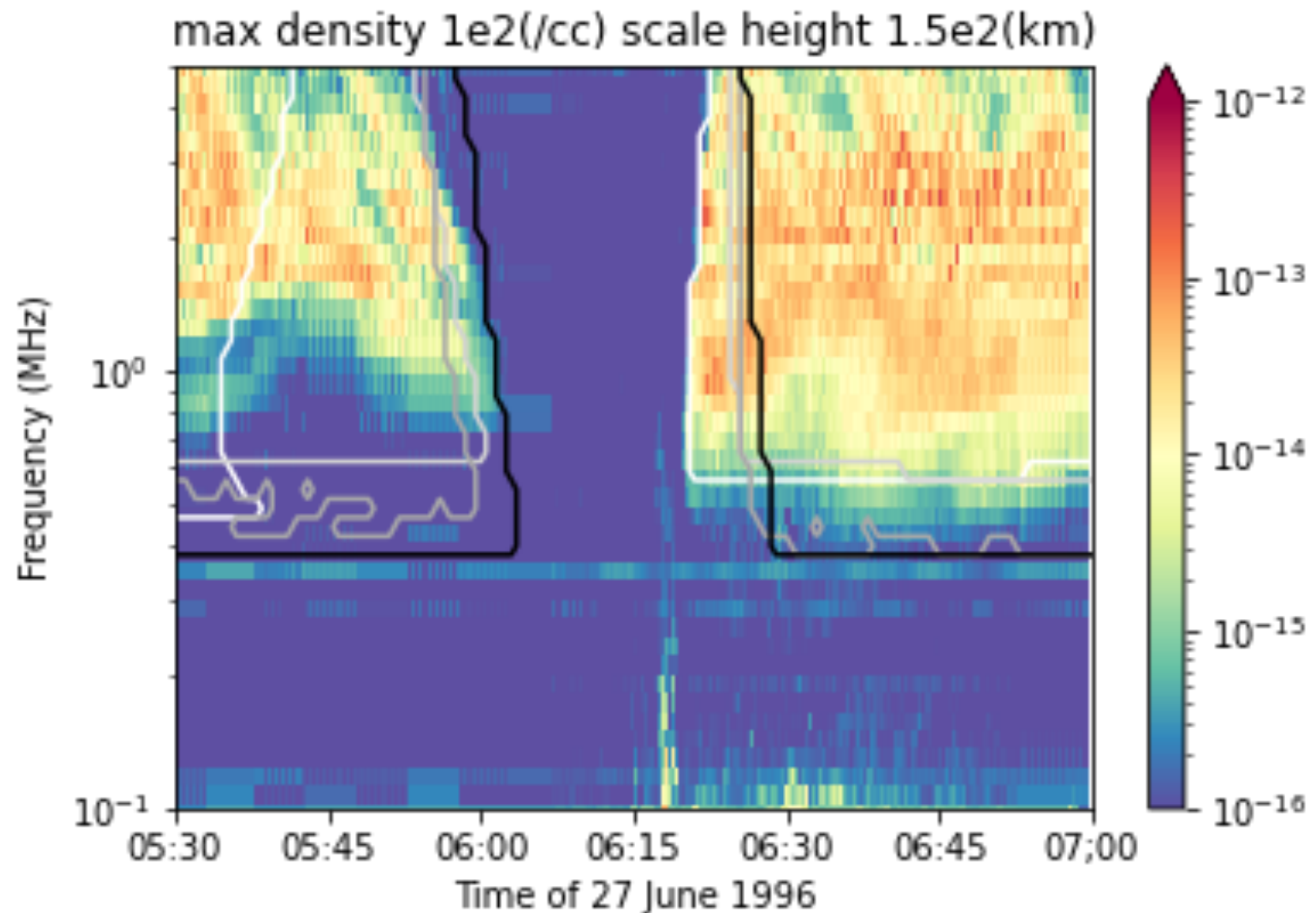


Fig.7 FTDT result [Principles of radar (Kazuo Ouchi)]

Ray tracing ..

more computationally efficient to trace propagation paths of electromagnetic waves in the magnetized plasma, sequentially solving the dispersion relation for plasma waves.



[For passive radar]

- We are going to simulate reflection and transmission of the EM waves in the ice crust and underlying ocean to explore their structures.
- Now I have already added reflective function on Europa's surface (Fig.22) and setting reflectance function (Fig.23).

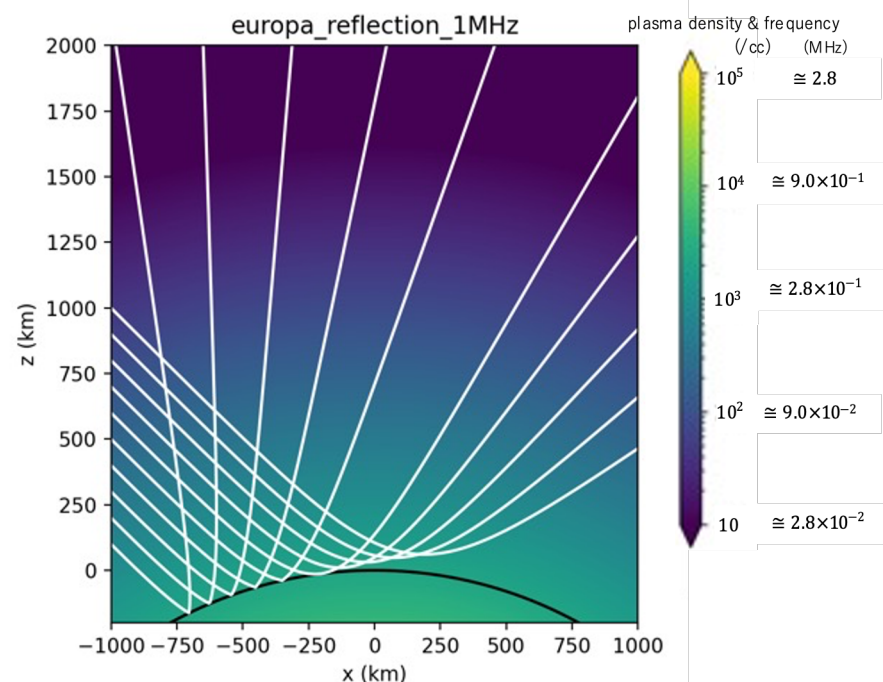


Fig.22 Surface reflection model of Europa

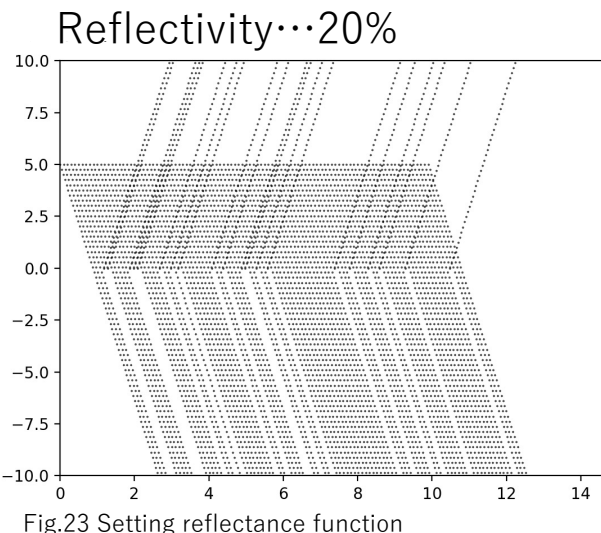
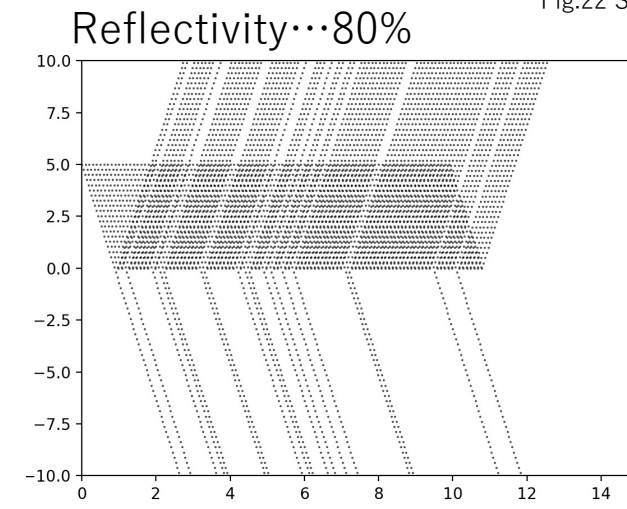
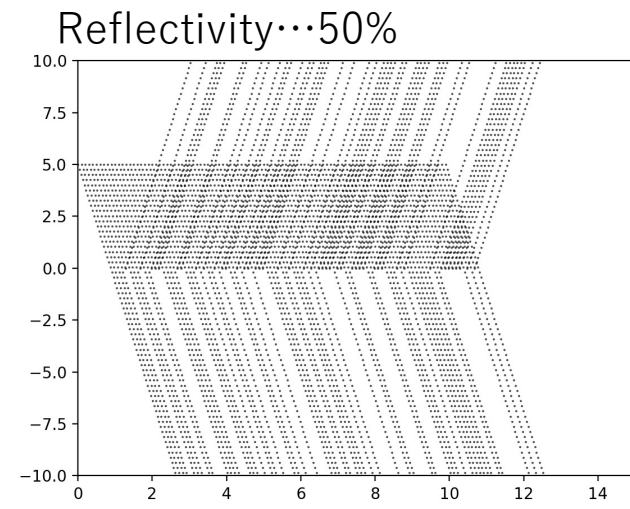


Fig.23 Setting reflectance function



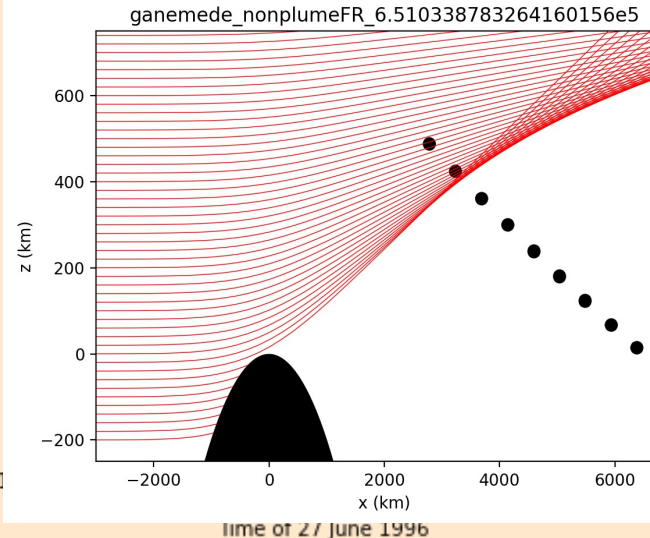
6.K –Why we can not distinguish?

44

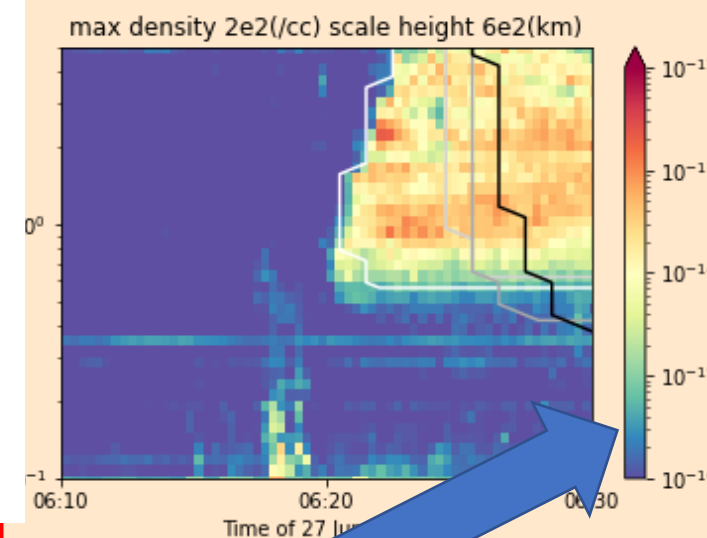
Refraction

Scale height

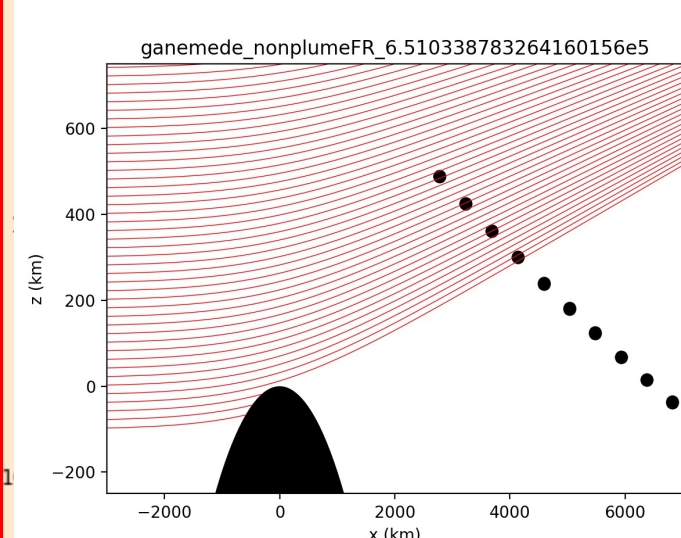
300 km



600 km

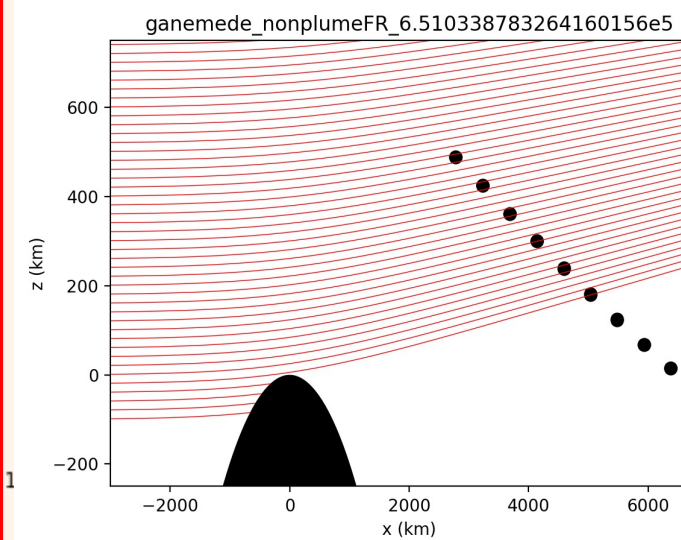
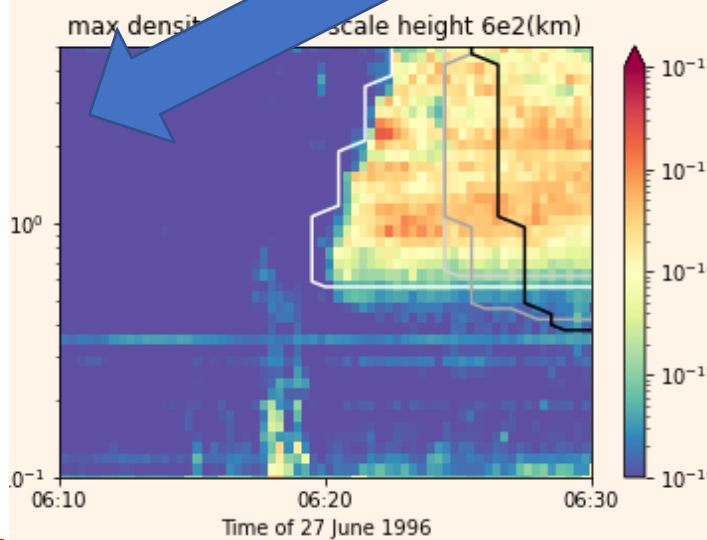
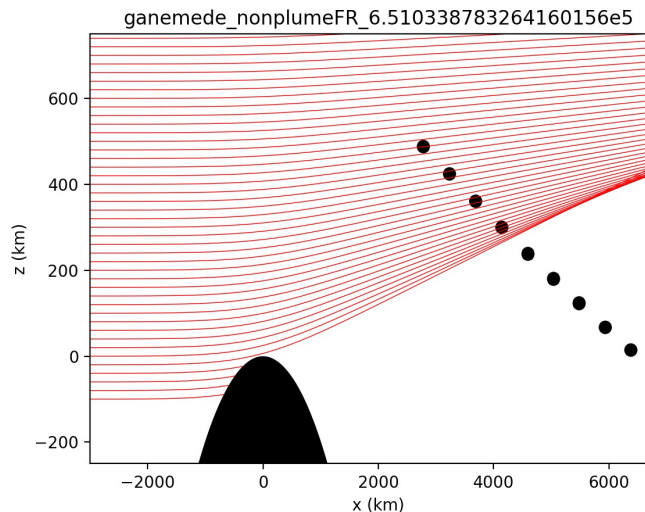


900 km



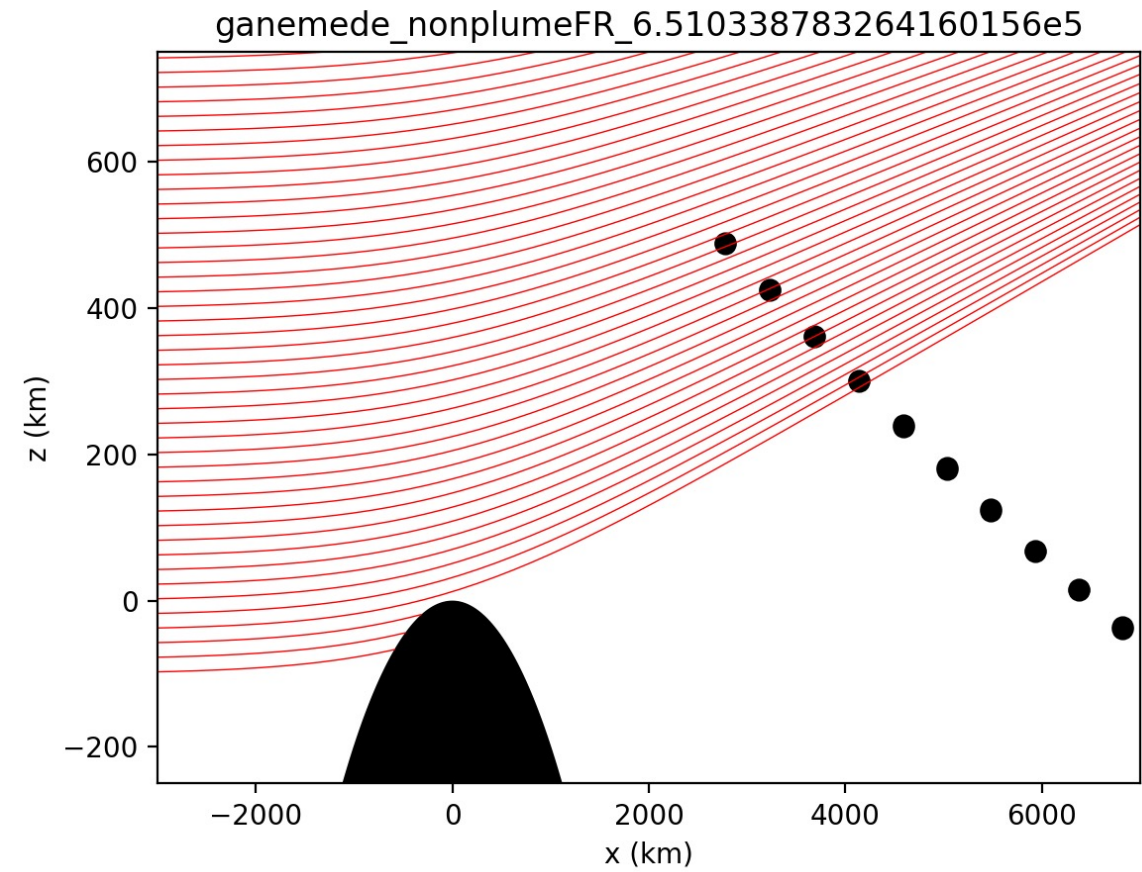
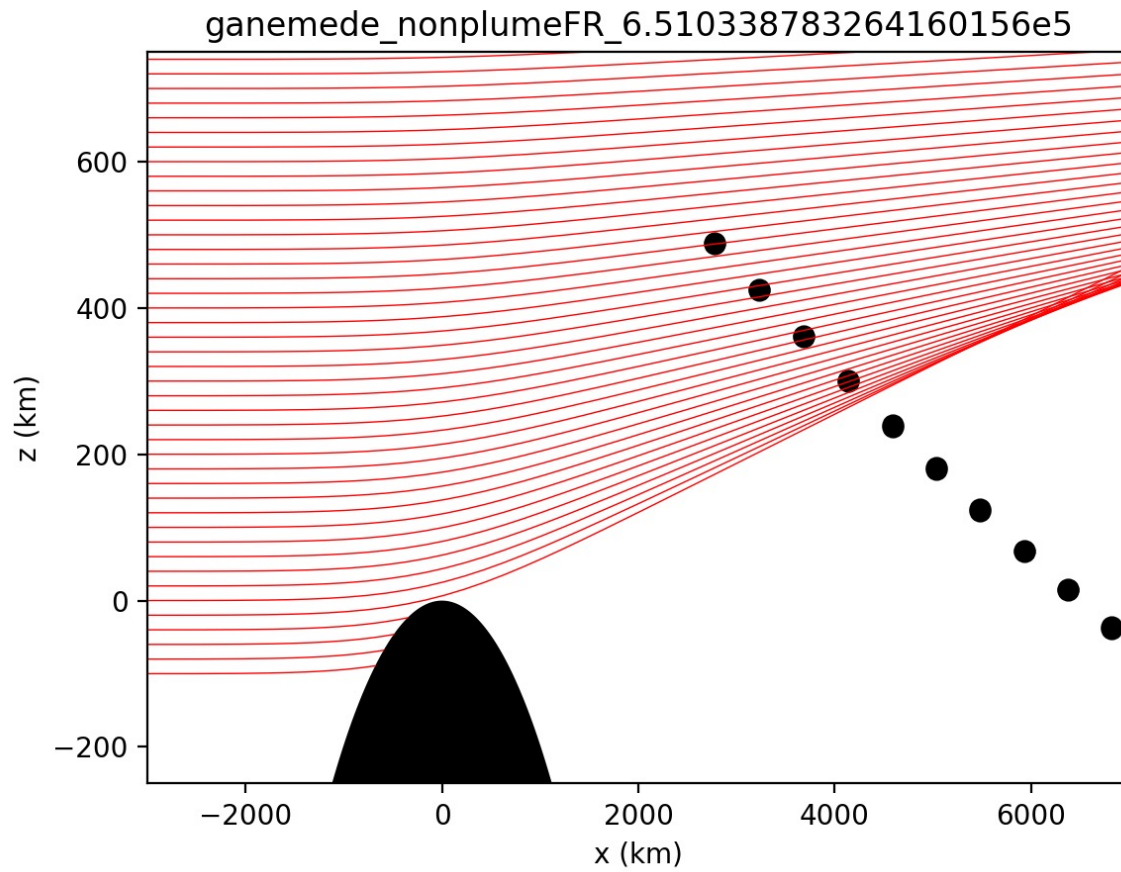
Max density

100 (/cc)



6.K –Why we can not distinguish?

45



ganymede_ingress_B_f-t_evaluate

